SKI Report 2006:17

Research

Three Dimensional Modelling of a KBS-3 Canister for Spent Nuclear Fuel – some migration studies

António Pereira

August 2006

ISSN 1104-1374
ISRN SKI-R-06/17-SE

SKI

SKI perspective

Background

As part of SKI's preparations for future license application to build a final repository for nuclear waste there is a need of examine the long term safety of the repository.

The canister and the surrounding bentonite have an important function to fulfill in order to prevent the radionuclides from reaching the environment. Situation may still occur where a pinhole (crack) may have arisen early in time in one or several canister(s). The radionuclides can then begin to be transported to the surrounding by the ground water through the pinhole in the canister farther into the bentonite and out into a fracture in the bed rock.

Usually simulation of radionuclide transports is done by introducing simplification of processes used in the model. The model is in most cases also one-dimensional.

Purpose

SKB includes in their one-dimensional model for radionuclide transport from a canister a process that arise in the transition between the pinhole in the canister and the bentonite and a process that arise in the transition between bentonite and the fracture in the surrounding bed rock. Both processes are interpreted as a resistance and simplified formulas are used. The assumptions of the transition processes that SKB have been used are described in their project SR 97 (SKB 1999).

To test the validity of using these "resistances" in SKB's one-dimensional compartment model, two three-dimensional model of the canister and its surrounding has been developed for each of these "resistances".

Results

It can be concluded from the 3D model simulations of the steady state resistance for the interface between pinhole and bentonite buffer that SKB's compartment modelling is a good approximation. A discrepancy exists whenever the cross-section of the pinhole is larger than about 1×10^{-4} m^2.

In respect to the resistance method for the interface between bentonite buffer and the fracture, the calculations indicates that the compartment modelling used by SKB's is slightly conservative. On the other hand, it is not trivial to verify if the dimensions and form of the fracture geometry used in the 3D model are in full consonance with the parameterisation given by the geometric factor in the compartment model used by SKB.

Effects on SKI work

Concerning the transport of radionuclides, from the pinhole in the canister, out to the bentonite one can be rather certain (for small pinholes) that SKB's model simplifications are valid. This is an important knowledge for SKI when reviewing SKB's safety analyses concerning the long term safety of a repository for spent fuel.

Future work

To investigate the validity of SKB's model simplifications for the transport of radionuclides from the bentonite buffer out to the fracture, another approach than the one of comparing "resistances" is needed. One way (suggested in the report) is to integrate the two 3D models into a single model of mass-transfer in the near field and compare the output fluxes with SKB's result in SR-97 report.

Project information

SKI reference: 14.9-040193/200409068 and SKI 2005/587-200509048.

Responsible at SKI has been Benny Sundström.

SKI Report 2006:17

Research

Three Dimensional Modelling of a KBS-3 Canister for Spent Nuclear Fuel – some migration studies

António Pereira

Department of Physics
AlbaNova University Center
Stockholm Center of Physics, Astronomy and Biotechnology
SE-106 91, Stockholm, Sweden

August 2006

Contents

Abstract

Performance assessment transport models use extensively the concept of transport resistance in the calculation of breakthrough curves of radionuclide releases in the near field and geosphere. The aim of this work is to examine more closely the applicability of the transport resistance approach. Can the resistance approach be used in for the estimation of fluxes through a pinhole of a defected canister? Or for the estimation of fluxes as given by the resistance of a fracture that crosses a canister hole? And if so, what is the degree of conservatism (if any) introduced by the use of that concept?

Two near-field 3D-models of the system consisting of canister, bentonite buffer and fracture have been developed. The goal is to examine the contribution to mass-transfer resistance of the interfaces between pinhole and bentonite buffer and between bentonite buffer and fracture respectively and to compare them with the resistance approach used by SKB in their compartment models of the near field.

For this purpose we have developed two 3D models using the FEMLAB® tool, to perform the set of calculations presented in this report. We estimate the above mentioned resistances separately for the interface between pinhole and bentonite buffer and for the interface between bentonite buffer and fracture respectively and we make a series of parameter variation studies.

We conclude that the pinhole resistance used by SKB is a good approach to be used by compartment models even if some small discrepancy exists whenever the cross-section of the pinhole is larger than 1×10^{-4} m^2. In respect to the fracture resistance parameterisation used in some SKB compartment models, the method is clearly conservative in many cases, with the exception for time points shorter than 200 years. This is due to the fact that the transient breakthrough curves cannot be described accurately by the parameterisation derived from the solution of the steady state equations used as the start point to deduce the transport resistance formulas. However definite conclusions on a quantitative level can only be obtained by integrating the two models developed during this work into a single integrated model of mass-transfer in the near field.

Sammanfattning

SKB's kompartmentmodeller använder sig av vissa massöverföringsapproximationer. De här approximationerna baseras på transportresistansbegreppet. I det här arbetet undersöker vi närmare, giltighetsområdet av transportresistansen. Kan transportresistansen användas för att uppskatta flödet från ett korrosionshål i en skadad kapsel? Eller för att beräkna flödet i en spricka i anslutning till en deponerad kapsel?

Två närområdesmodeller i 3D av ett system bestående av kapsel, bentonitbuffert och spricka har utvecklats. Syftet är att undersöka bidraget till massöverföringsresistansen från gränssnittet mellan korrotionshål och bentonitbuffert och mellan bentonitbuffert och spricka och jämföra de med resistansbegreppet som SKB använder i sina kompartmentmodeller.

För det här ändamålet har vi utvecklat två separata 3D modeller med hjälp av FEMLAB® och gjort en serie beräkningar som presenteras i detta arbete. Vi har uppskattat var för sig, resistansen vid gränssnittet mellan korrosionshål i en kapsel och bentonitbuffert och mellan bentonitbuffert och spricka i berget dvs. vid ingången till en spricka i berget. Vi har också gjort en serie av parametervariationsstudier.

Den viktigaste slutsatsen är att resistansen utav ett korrosionshål såsom används av SKB i sina kompartmentmodeller är en god approximation, även om små diskrepanser inträffar för hål som har ett tvärsnitt större än 1×10^{-4} m^2.

När det gäller parameteriseringen av sprickresistansen i SKB's modeller, är metoden något konservativ i många fall, med undantag för perioder kortare än 200 år. Det beror på att den initiala delen av de tidsberoende utsläppskurvorna inte kan beskrivas noggrant med parameteriseringar härledda från den stationära ekvationen som är startpunkten för att härleda formlerna för resistansen. Definitiva slutsatser på en kvantitativ nivå kan bara göras genom att integrera de båda modellerna, till en enda massöverföringsmodell för närområdet.

1 Introduction

The near-field (canister and deposition-hole scale) model used by SKB for spent fuel disposal assessments utilises several mass-transfer approximations. Transport resistances are used to represent the release of radionuclides from a copper canister through a pinhole and to represent transfer from the bentonite buffer to a water-bearing fracture in the host rock (Hedin, 2002, Lindgren and Lindström, 1999, SKI/SSI, 2003).

The mass-transfers through these narrow interfaces play a critical role in determining the near-field release and hence the calculated doses.

In this Section we specify a series of calculations to evaluate the validity of the transport resistance methods employed by SKB. We focus on the key interfaces, but these could potentially be relaxed in later studies.

The most direct approach would be to model the canister, bentonite buffer and fracture system as a whole. However, this approach has two weaknesses: it makes a direct evaluation of the equivalent mass-transfer coefficients difficult; and it could be computationally overly complex. Thus, in this work we study the two interfaces separately.

The geometry of the system is that used in SR97 (Hedin, 2002 and Lindgren and Lindström, 1999), as illustrated in Figure 2.1.1. We are investigating the path Q1 (direct release into a fracture intersecting the canister deposition hole) considered in SR97, and so can ignore transport through the top or bottom of the bentonite buffer. Inside the canister we will assume a uniform concentration. Two situations are considered. In one case, this concentration is fixed for all time (representing a solubility-limited nuclide); in the other case, the initial inventory in the canister is fixed and the concentration falls as nuclides are released (representing a gap-release radionuclide). Radioactive decay and ingrowth can be ignored for this study. The system is fully saturated at all times (gas produced in the can that might complicate the release is not considered here).

2 Case specifications

2.1 Pinhole interface

Three dimensional modelling

The pinhole is assumed to penetrate the full canister thickness (Figure 2.1.1). Its cross-sectional shape is taken to be square. The pinhole will be considered to be full of water in the base case (PW), but a variant where it is partially full of bentonite is also considered (PB).

When looking at the pinhole case, the model stops at the edge of the bentonite buffer. A "mixing cell" condition is imposed at the interface between pinhole and bentonite buffer – balancing the diffusive flux with advection through the host rock (assumed to be uniformly distributed). This comes down to a linear combination of the boundary concentration and gradient being zero (se Section 6.1).

In the bentonite buffer, linear equilibrium sorption is assumed.

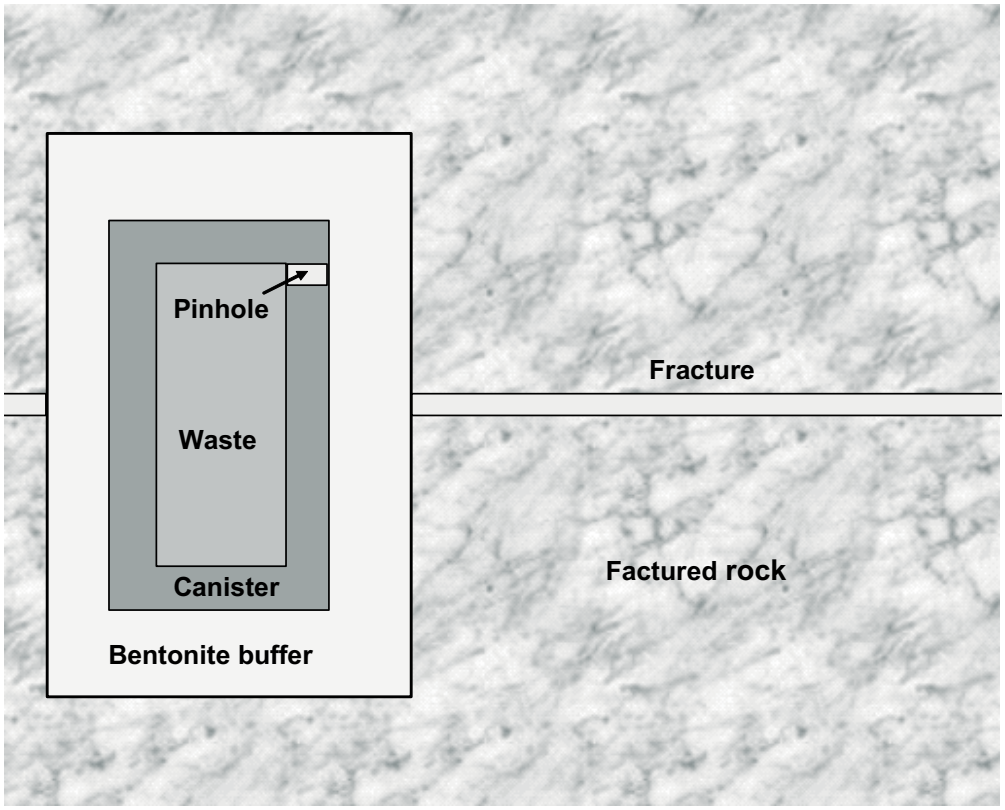

Figure 2.1.1 System geometry.

Data requirements and the calculation cases are shown in Tables 2.1.1 and 2.1.2 respectively. The data on water diffusivity, bentonite diffusivity and sorption coefficients are taken from Hedin (Hedin, 2002). These data come originally from many

of the cases analysed in the assessment of the KBS 3 repository (SKB 1999). The data variations, for instance the values of the sorption coefficient Kd, labelled with KdL (low Kd), KdM (medium Kd) and KdH (high Kd) of Table 2.1.1 cover the expected input uncertainty of the sorption coefficient. Our use of the data from 27 cases used by Hedin (Hedin 2002) and the combinations of it to construct the cases of Table 2.2.2 covers reasonably input data uncertainty and variability used in the KBS-3 repository work. Hedin uses mainly generic data from case 4.2.1 of the SR-97 report (Lindgren and Lindström, 1999). The cross-section dimensions of the pinhole changes suddenly from 1×10^{-6} m^2 to 1×10^{-2} m^2 at 20,000 years in Hedin´s work. We have chosen to study the impact of the variation of the cross-section from 1×10^{-6} m^2 to 1×10^{-2} m^2 in steps of one order of magnitude (A1 to A5 in Table 2.1.1). The source term represents either a solubility limited nuclide of one unit concentration or a unit inventory (UC=1 or UI=1 respectively, in Table 2.1.1).

Table 2.1.1 *Selected Data for the Pinhole Interface.*

Data Item	Data source and variations	Variables
Source term	Solubility limited nuclide of one unit concentration Unit inventory	 UC=1 UI=1
Canister Water Volume	From SR97 - 1 m^3	
Pinhole area	SR97 jumps from 1×10^{-6} m^2 to 1×10^{-2} m^2. Take a series of values:	A1=1×10^{-6} m^2 A2=1×10^{-5} m^2 A3=1×10^{-4} m^2 A4=1×10^{-3} m^2 A5=1×10^{-2} m^2
Pinhole content	Water with variant 50% bentonite (i.e. outer 50% all bentonite)	PW (water in pinhole)=1 PB (50% bentonite)=0.5
Water effective diffusion coefficient	SR97 value (3.2×10^{-2} m^2 y^{-1})	
Bentonite buffer effective diffusion coefficient	SR97 value for Se (2.2×10^{-3} m^2 y^{-1}) Variant up and done by factor 10	DM (SR97) =2.2×10^{-3} m^2 y^{-1} DL (low) =2.2×10^{-4} m^2 y^{-1} DH (high) =2.2×10^{-2} m^2 y^{-1}
Bentonite buffer sorption	SR97 value for Tc (0.1 m^3 kg^{-1}) Variant up and done by factor 100	KdM (SR97) =0.1 m^3 kg^{-1} KdL (low) =0.001 m^3 kg^{-1} KdH (high) =10 m^3 kg^{-1}
Boundary conditions	to be specified from SR97 Darcy velocity values (2×10^{-3} m y^{-1})	

Note: Other data can be found in Hedin (2002) and Lindgren and Lindström (1999).

Table 2.1.2 *Calculation Cases for the Pinhole Interface.*

Case	Canister Concentration	Pinhole Area	Pinhole Content	Bentonite buffer effective Diffusion coefficient	Bentonite buffer Sorption
1	UI	A1	PW	DM	KdM
2	UI	A1	PW	DL	KdM
3	UI	A1	PW	DH	KdM
4	UI	A1	PW	DM	KdL
5	UI	A1	PW	DM	KdH
6	UI	A1	PB	DM	KdM
7	UI	A1	PB	DL	KdM
8	UI	A1	PB	DH	KdM
9	UI	A1	PB	DM	KdL
10	UI	A1	PB	DM	KdH
11	UI	A2	PW	DM	KdM
12	UI	A3	PW	DM	KdM
13	UI	A4	PW	DM	KdM
14	UI	A5	PW	DM	KdM
15	UI	A2	PB	DM	KdM
16	UI	A3	PB	DM	KdM
17	UI	A4	PB [1]	DM	KdM
18	UI	A5	PB [1]	DM	KdM
19	UC	A1	PW	DM	KdM
20	UC	A1	PW	DM	KdL
21	UC	A1	PW	DM	KdH
22	UC	A1	PB	DM	KdM
23	UC	A2	PW	DM	KdM
24	UC	A3	PW	DM	KdM
25	UC	A3	PB	DM	KdM
26	UC	A4	PB [1]	DM	KdM
27	UC	A5	PB [1]	DM	KdM

[1] 100% bentonite assumed.

Compartment modelling by SKB

The three dimensional calculation cases are compared with a compartmental model of the same system using the SKB mass-transfer coefficient. The transfer resistance used for the interface between the canister and the pinhole (Hedin, 2002) is:

$$\Omega = \frac{d_{Hole}}{D\, A_{Hole}} \tag{2.1}$$

where d_{Hole} is the length of the hole, A_{Hole} its area and D is the effective diffusivity in water. The resistance for the interface between pinhole and bentonite buffer was taken as:

$$\Omega = \frac{1}{D\sqrt{2\pi\, A_{Hole}}} \qquad (2.2)$$

2.2 Fracture interface

Three dimensional modelling

The fracture is assumed to be planar. The aperture is fixed and flow in the fracture is controlled by a specified pore velocity at distance and by the impermeable bentonite buffer (acting as a no flow condition). Two source terms are considered: in one case the concentration is fixed at the canister (labelled with CC in Table 2.2.1); in the other there is an initial uniform concentration in the bentonite buffer (labelled with BI in Table 2.2.1). In the bentonite buffer, linear equilibrium sorption will be assumed. The data requirements and combination of calculation cases are shown in Table 2.2.1 and 2.2.2 respectively.

Table 2.2.1 *Selected Data Requirements for the Fracture Interface.*

Data Item	Data source and variations	Variables
Source term	Unit concentration at canister Unit inventory in bentonite buffer	CC=1 BI=1
Bentonite buffer effective diffusion coefficient	SR97 value for Se (2.2×10^{-3} $m^2\,y^{-1}$) Variant up and down by factor 10	DM (SR97) =2.2×10^{-3} $m^2\,y^{-1}$ DL (low) =2.2×10^{-4} $m^2\,y^{-1}$ DH (high) =2.2×10^{-2} $m^2\,y^{-1}$
Bentonite buffer sorption	SR97 value for Tc (0.1 $m^3\,kg^{-1}$) Variant up and done by factor 100	KdM (SR97) =0.1 $m^3\,kg^{-1}$ KdL (low) =0.001 $m^3\,kg^{-1}$ KdH (high) =0 $m^3\,kg^{-1}$
Pore velocity	Calculated form Darcy velocity, assuming one fracture takes all the flow for the canister	
Darcy velocity	SR97 case (2×10^{-3} m y^{-1}) with higher and lower by factors of 2 and 10	VM (SR97) =2×10^{-3} m y^{-1} VL2 VL10 =1×10^{-3} 2×10^{-4} m y^{-1} VH2 VH10 =4×10^{-3} 2×10^{-2} m y^{-1}
Aperture	SR97 case (1×10^{-4} m) with larger and smaller by factor 10	HM (SR97) =1×10^{-4} m HL =1×10^{-3} m HS =1×10^{-5} m
Diffusion in water in the fracture	SR97 value (3.2×10^{-2} $m^2\,y^{-1}$)	
Boundary condition	Zero concentration upstream some distance (on inflow boundaries); zero gradient downstream some distance (on outflow boundaries)	

Note: Other data can be found in Hedin (2002) and Lindgren and Lindström (1999).

Table 2.2.2 *Calculation Cases for the Fracture Interface.*

Case	Source	Bentonite Buffer Diffusion	Bentonite Buffer Sorption	Darcy Velocity	Fracture Aperture
1	BI	DM	KdM	VM	HM
2	BI	DL	KdM	VM	HM
3	BI	DH	KdM	VM	HM
4	BI	DM	KdL	VM	HM
5	BI	DM	KdH	VM	HM
6	BI	DM	KdM	VL2	HM
7	BI	DM	KdM	VL10	HM
8	BI	DM	KdM	VH2	HM
9	BI	DM	KdM	VH10	HM
10	BI	DM	KdM	VM	HL
11	BI	DM	KdM	VL2	HL
12	BI	DM	KdM	VL10	HL
13	BI	DM	KdM	VH2	HL
14	BI	DM	KdM	VH10	HL
15	BI	DM	KdM	VM	HS
16	BI	DM	KdM	VL2	HS
17	BI	DM	KdM	VL10	HS
18	BI	DM	KdM	VH2	HS
19	BI	DM	KdM	VH10	HS
20	CC	DM	KdM	VM	HM
21	CC	DL	KdM	VM	HM
22	CC	DH	KdM	VM	HM
23	CC	DM	KdH	VM	HM
24	CC	DM	KdM	VL2	HM
25	CC	DM	KdM	VH2	HM
26	CC	DM	KdM	VM	HL
27	CC	DM	KdM	VL2	HL
28	CC	DM	KdM	VH2	HL
29	CC	DM	KdM	VM	HS
30	CC	DM	KdM	VL2	HS
31	CC	DM	KdM	VH2	HS

Compartment modelling by SKB

The three dimensional calculation cases are compared with a compartmental model of the same system using the SKB transfer resistance approach. The flow transfer resistance used for the interface between the bentonite buffer and the fracture is given by (Hedin, 2002):

$$\Omega = \frac{1}{A_q \sqrt{q}} \qquad (2.3)$$

where A_q is a lumped parameter with a value of 0.03 $m^{2.5}/ y^{0.5}$ for the reference parameters used for the pathway into a fracture intersecting the deposition hole. The

fracture is located adjacent to the pinhole on the canister wall (transport path Q1 in ref. SKB, 1998) and q is the near-field Darcy flux (taken to have a value of 0.002 m y^{-1}). An additional resistance was added to the flow resistance given by:

$$\Omega = \frac{B}{D} \tag{2.4}$$

where B is another lumped parameter with dimensions m^{-1}. For transport path Q_1 with the reference parameters this has a value of 0.9 m^{-1}. D is here the effective diffusivity for bentonite buffer.

3 Modelling Geometry

The 3D geometry of our system is represented using domain decomposition. The aim of this approach is to enhance the grid quality while keeping the number of degrees of freedom within a reasonable range. In this way we can reduce the CPU burden of the FEM calculations and speed up the simulation time.

The domain decomposition implies that we divide the geometry in independent regions and therefore we have separated grids one for each region. The physical equations operating on each region are coupled to each other at the interfaces common to the respective regions.

The physical dimensions of the near field barrier system are given in Table A1 of Appendix II.

3.1 Pinhole Interface

We use the symmetry of the problem to model only one half of the geometrical domain. The 3D geometry used to simulate the pinhole interface cases is shown in Figures 3.1.1 to 3.1.4. The geometry is decomposed in five regions (Table 3.1.1)

Table 3.1.1 *The domain decomposition of the geometry.*

Region	Description
1	Bentonite buffer below the canister.
2	Bentonite buffer above the canister.
3	Canister interior with water filled gap.
4	Pinhole[a].
5	Bentonite buffer surrounding the canister.

[a] The pinhole is dived in two equal regions. In a few of the case studies, half of the pinhole is filled with bentonite and half with water.

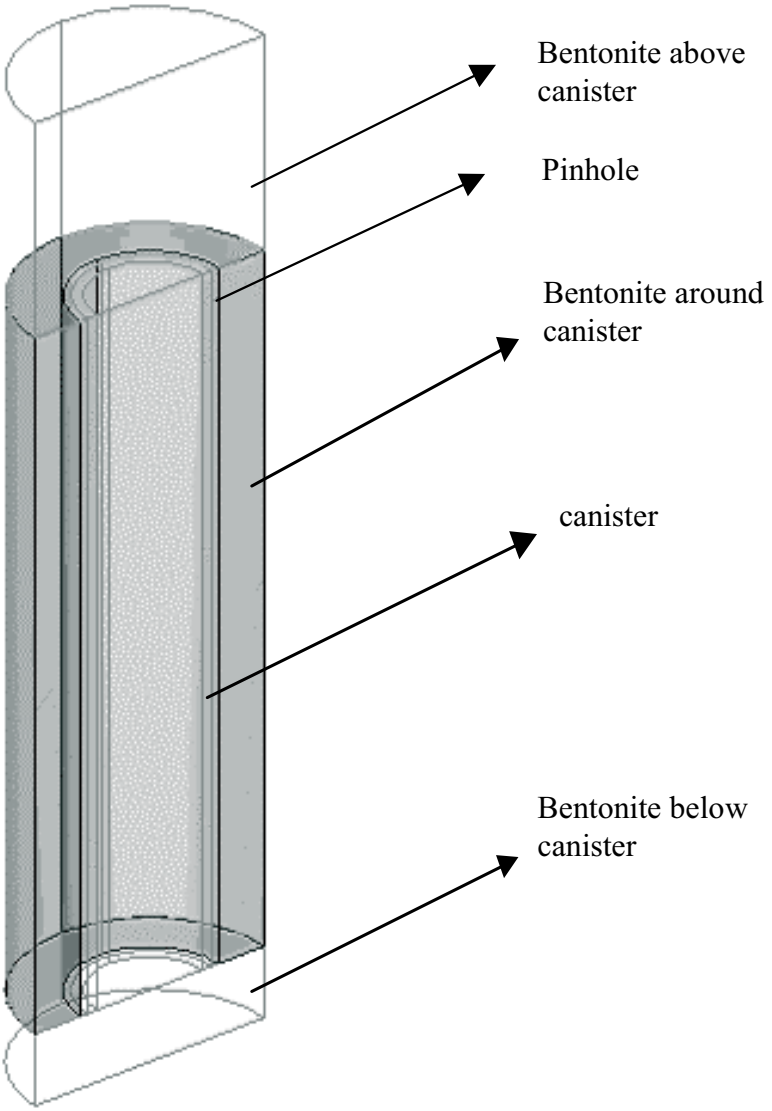

Figure 3.1.1 *The domain geometry of the pinhole-interface model.*

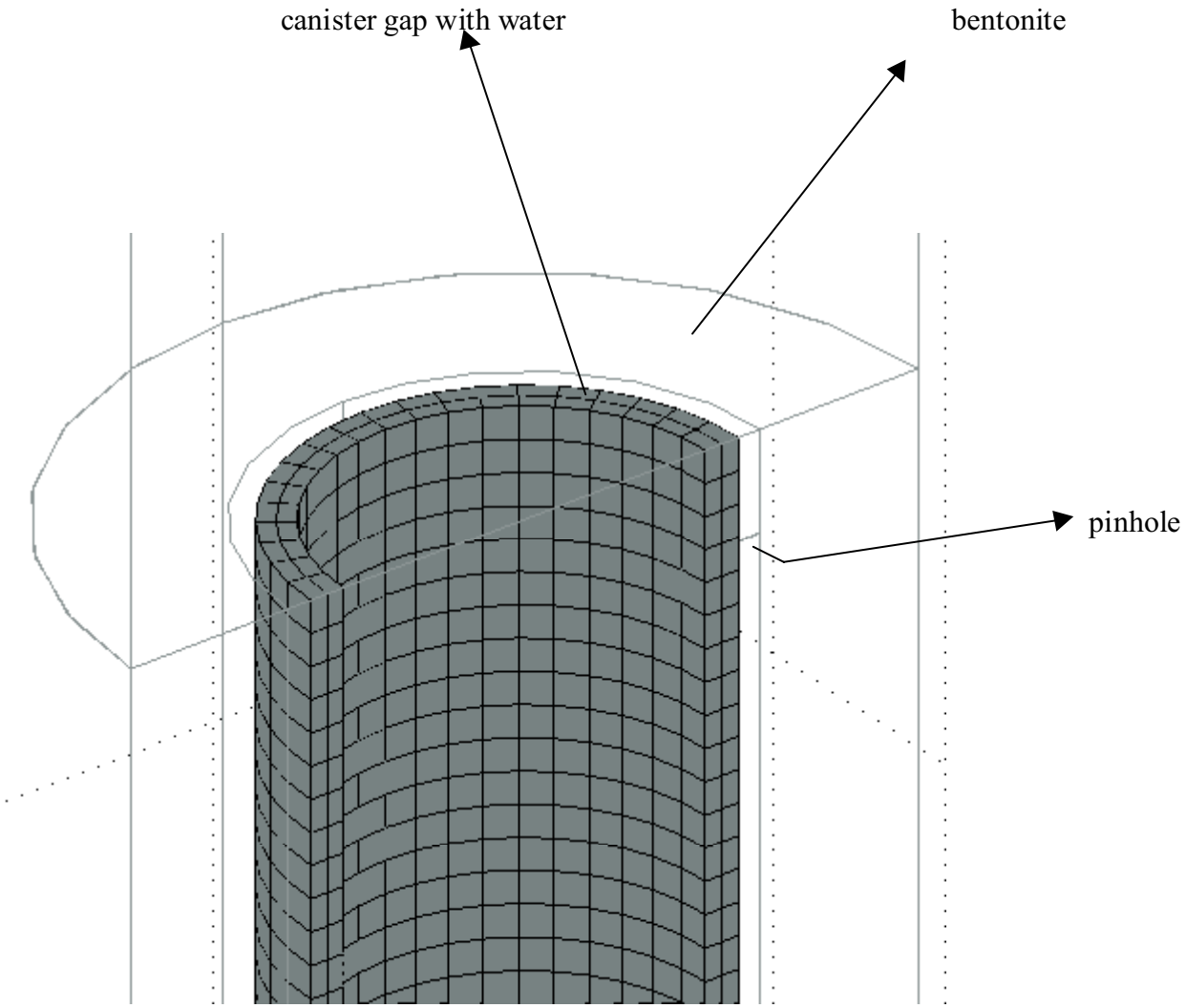

Figure 3.1.2 *The region meshed is a partial view of the water filled gap in the interior of the canister, region 3.*

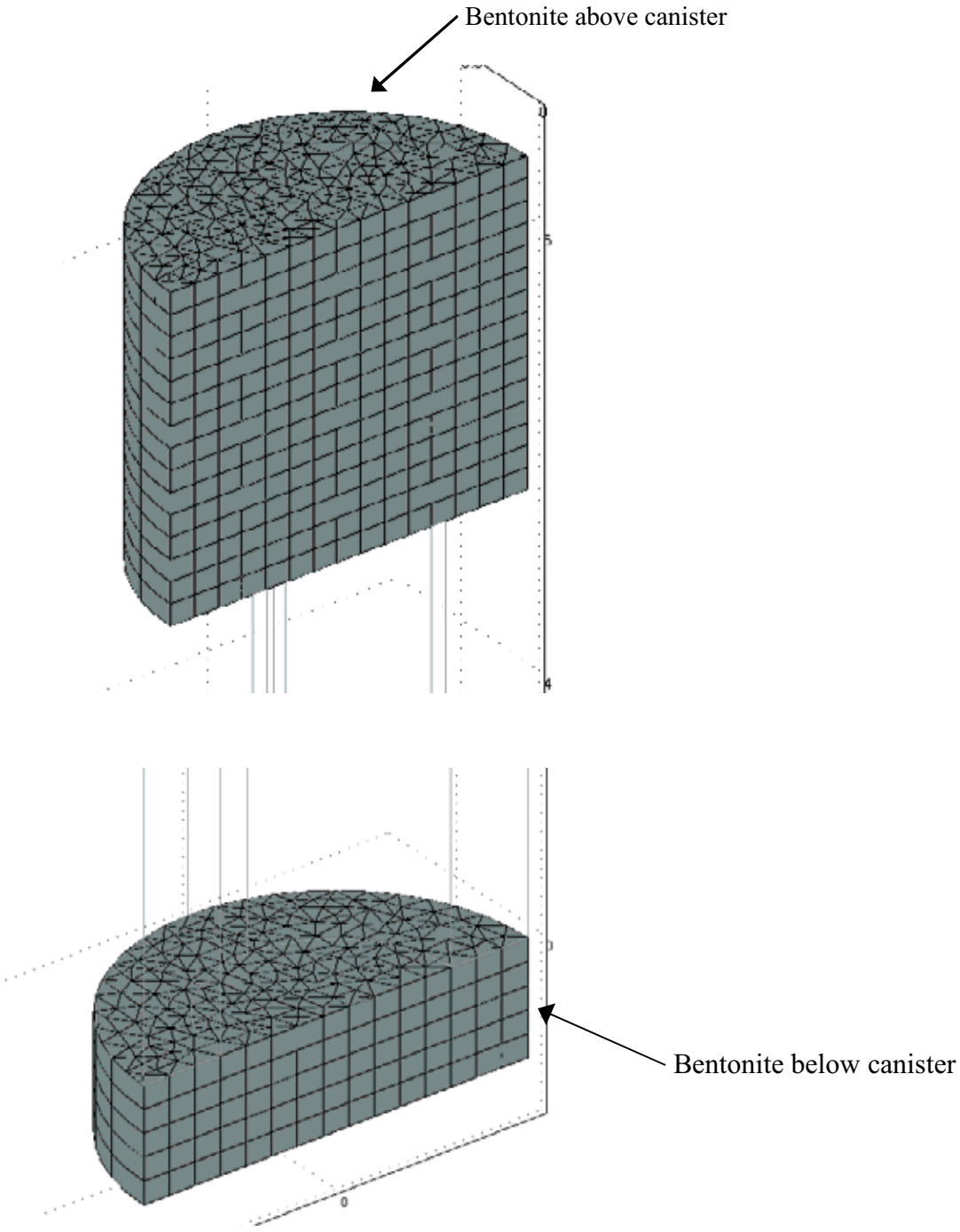

Figure 3.1.3 *The meshed regions show the bentonite buffer above the canister (upper picture, region 2) and the bentonite buffer bellow the canister (lower picture, region 1).*

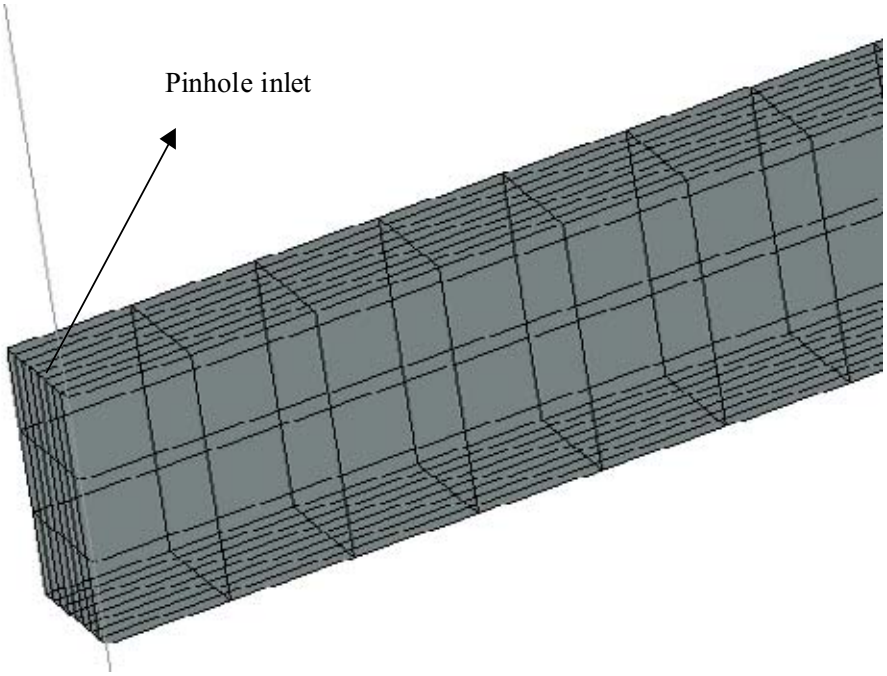

Figure 3.1.4 *The meshed region is a partial view of the pinhole, region 4.*

3.2 Fracture Interface

The 3D geometry used to simulate the fracture interface cases is shown in Figure 3.2.1. In this case the geometry is divided in four regions (Table 3.2.1). The fracture has a small aperture. It can be as low as five orders of magnitude lower than that of the canister height (the smallest aperture is 1×10^{-5} m), which makes the modelling far from trivial. In this case the use of domain decomposition is essential to solve the problem. In Figure 3.2.1 the other regions are shown in blue. Figure 3.2.2 shows the mesh of the fracture.

Table 3.2.1 *The domain decomposition of the fracture interface geometry.*

Region	Description
1	Bentonite buffer below the canister.
2	Bentonite buffer above the canister.
3	Bentonite buffer surrounding the canister
4	Rock fracture intercepting the canister hole

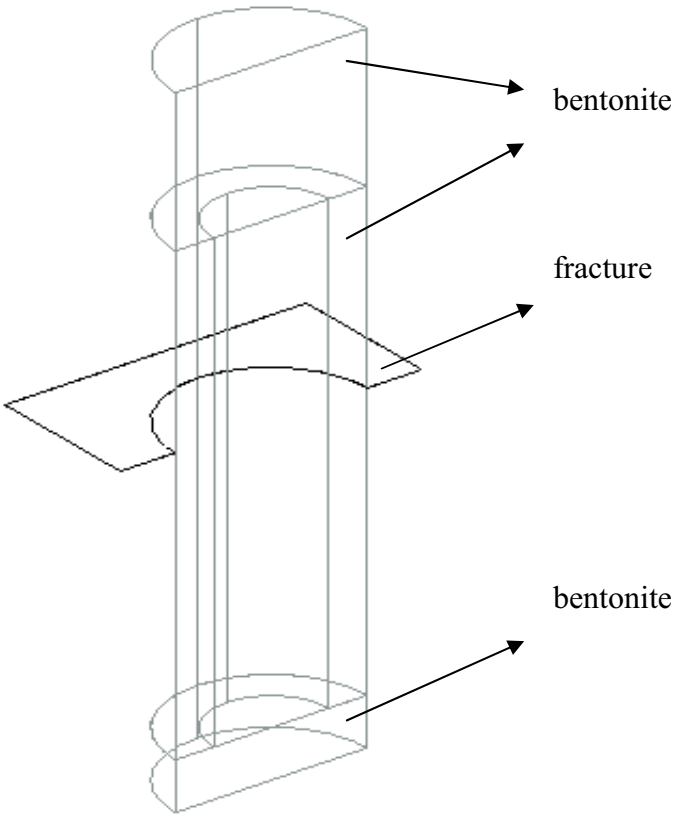

Figure 3.2.1 *The plane fracture intercepting the canister hole.*

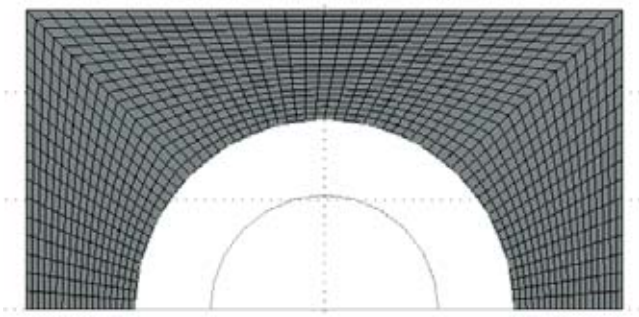

Figure 3.2.2 *The mesh of the fracture intercepting the canister hole.*

4. Domain equations

4.1 Pinhole Interface

This case is controlled by diffusion. The system is described by a system of coupled partial differential equations, modelling the time-dependent radionuclide transport:

$$K_{vol}\frac{\partial c_i}{\partial t}+\nabla\cdot(-D_{eff,i}\cdot\nabla c_i)=0 \tag{4.1}$$

with

$$K_{vol}=\varepsilon+(1-\varepsilon).\rho.K_d \tag{4.2}$$

where:

$c_i\,(x,y,z,t)$ - is the concentration in region *i* (*i = 1,2 ...5*),
$D_{eff,\,i}\,(x,y,z)$ - is the effective diffusivity in region *i,*
$\rho\,(x,y,z)$ - is the density of bentonite,
K_d - is the distribution coefficient of region *i,*
ε - is the porosity of the bentonite,
$K_{vol}\,(x,y,z)$ - is the capacity factor of the bentonite.

4.2 Fracture Interface

This model is described by a system of partial differential equations, representing the advection and diffusion in the bentonite buffer and fracture (Equation 4.3a) coupled to the Navier-Stokes equation combined with the continuity equation (Equation 4.3b). The water flow is in the fracture is first calculated by the Navier-Stokes equation. Once the steady-state velocity field is obtained we can use it in the advection-diffusion equation to calculate the concentrations in the different domains and the resulting fluxes.

$$R_i\frac{\partial c_i}{\partial t}+\nabla\cdot(-D_i+c_i\,\mathbf{u}_i)=0 \tag{4.3a}$$

$$\begin{cases}-\nabla.\eta\,(\nabla\mathbf{u}+(\nabla\mathbf{u})^{\mathrm{T}})+\rho(\mathbf{u}.\nabla)\mathbf{u}+\nabla\mathrm{p}=0\\ \nabla\cdot\mathbf{u}=0\end{cases} \tag{4.3b}$$

where

R_i - is the retardation coefficient of the fracture,
$c_i\,(x,y,z,t)$ - is the concentration in region *i* (*i = 1,2 ...5*),
$D_i\,(x,y,z)$ - is the effective diffusivity in region *i*,

u - is the advective velocity in the fracture,
η - is the water viscosity,
ρ - is the water density,
p - is pressure.

We assume no retardation in the fracture (R=1).

5 Boundary conditions

5.1 Pinhole Interface

For the pinhole interface calculations the effect of the rock is mimic with the help of the boundary conditions at the interface between the bentonite buffer and the rock. Those boundary conditions are obtained in the following way. We balance the diffusive flux out of the bentonite buffer with the advective flux in the rock. This is done on an average basis, so that a local condition can be used.

If the average concentration just outside the bentonite buffer is C_{av} then the advective flux can be approximated as

$$F_{adv} = 2\,R\,L\,q\,C_{av} \tag{5.1}$$

where we assume that the relevant flow through is that through the rock over an area equal to the cross-sectional area of the bentonite buffer. The diffusive flux from the bentonite buffer (again taking an average) is

$$F_{diff} = -2\,\pi\,R\,L\,D\left.\frac{\partial C_{ave}}{\partial r}\right|_{r=R} \tag{5.2}$$

Balancing these fluxes locally at all points on the surface gives

$$\left[2\,R\,L\,q\,C + 2\,\pi\,R\,L\,D\frac{\partial C}{\partial r}\right]_{r=R} = 0$$

that is[1]

$$\left[q\,C + \pi\,D\frac{\partial C}{\partial r}\right]_{r=R} = 0 \tag{5.3}$$

with:

D - bentonite buffer diffusion coefficient,
R - outer radius of bentonite buffer,
L - vertical height of bentonite buffer,
q - Darcy velocity in the host rock.

5.2 Fracture Interface

We assume that initially, the concentration in the fracture is zero (Figure 5.2.1). A conservative trace penetrates the fracture surrounding the bentonite buffer through the

[1] Equation (5.3) was derived by Peter Robinson, Quintessa Ltd.

common boundary between the bentonite buffer and the fracture and is transported downwards by the flow in the fracture. At the outlet, the gradient of the concentration is nil. At the interface between the bentonite buffer and the fracture we have for the flow, a no slip boundary condition.

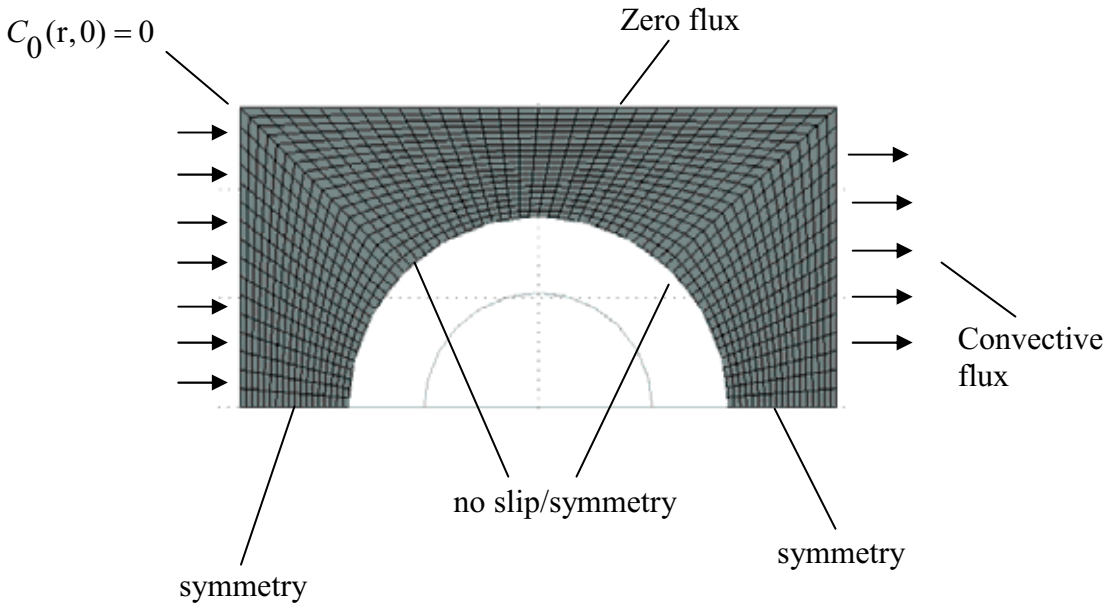

Figure 5.2.1 *Boundary conditions of flow and mass transport in the fracture.*

6 Results and Discussion

We have solved first, the steady state problem, in order to compare the resistance in the three dimensional modelling with SKB's compartment modelling. Then we compare the three dimensional steady state results with those of the full transient calculations that give the breakthrough curve as a function of time.

In the transient calculations the solution converges with relative and absolute numerical tolerances equal to 10^{-7} and 10^{-8} respectively. The convergence of the solver was checked by refining the mesh and by increasing the tolerances, until the obtained concentrations were shown to be stable.

6.1 Pinhole Interface Calculations

6.1.1 Steady state

We have calculated the concentrations at the inlet and outlet of the pinhole, $C_{w/p}$ and $C_{p/b}$ respectively. The subscripts in $C_{w/p}$ and $C_{p/b}$ stand for the interface between waste and pinhole and the interface between pinhole and bentonite buffer respectively. The flux at the outlet of the pinhole, φ, was also calculated. It is the flux of material (mole/s) between the pinhole and the bentonite buffer.

Compartment modelling by SKB

The resistance of the pinhole to the transport of nuclides by diffusion (Hedin 2002) is given by Equation 6.1:

$$R_{pinhole} = \frac{l}{A\, D_{eff}} \tag{6.1}$$

where l (m) is the length of the pinhole, A (m^2) is the area of the pinhole cross-section, D_{eff} is the effective diffusivity of the water in the pinhole. Equation (6.1) is an approximation derived from the two-dimensional analytic solution of the steady state diffusion equation and is for a small pinhole of circular cross-section filled with water. To compute the flux at the interface between the pinhole and the bentonite buffer, a new additional resistance must be taken into account if a compartment model is used.

The resistance offered by the interface between the pinhole and the bentonite buffer is (Hedin, 2002)

$$R_{p/b}^{diff} = \frac{1}{D_{eff}^{b}\sqrt{2\pi A}} \tag{6.2}$$

where D_{eff}^{b} is the effective diffusivity in the bentonite buffer and A is the pinhole cross--section area. The total resistance of the pinhole and bentonite buffer is therefore R_{SKB}:

$$R_{SKB} = R_{pinhole} + R_{p/b}^{diff} \tag{6.3}$$

Three dimensional modelling

Using the FEMLAB calculation we can compute the transport resistance R by evaluating the computed flux and the concentrations at the inlet and outlet of the pinhole:

$$R = \frac{\Delta C}{\varphi} = \frac{C_{w/p} - C_{p/b}}{\varphi} \tag{6.4}$$

where φ (mole/s) is the flux at the interface between the canister and the bentonite buffer (outlet of the pinhole). $C_{w/p}$ (mole/m^3) is the concentration at the interface between the waste and the pinhole (inlet concentration) and $C_{p/b}$ (mole/m^3) is the concentration at the interface between the pinhole and bentonite buffer (outlet concentration).

Results of calculations

The evaluation of the release rate from the pinhole of Case 19, is used here to illustrate the pinhole interface model and the computational approach. The case assumes a constant concentration in the interior of the canister.

The results of the steady state calculations of the three dimensional modelling for the case are:

φ = 2.021013×10^{-14} (mole/s),
$C_{p/b}$ = 3.741×10^{-3} (mole/m^3),
$C_{w/p}$ = 0.999592 (mole/m^3).

Using Equation 6.4 we get for the compartment modelling the resistance:

$R = 4.93\times10^{13}$ (s/m^3).

From Equation (6.3) we get R_{SKB}= 4.9275×10^{13} +$5.7187\cdot10^{12}$ =5.50×10^{13} (s/m^3) for the compartment modelling.

The numerical result of the pinhole resistance of the three dimensional modelling agrees satisfactory with that given by the equation used by SKB. We should note that the $R_{pinhole}$ term of Equation (6.3) agrees exactly with R value of Equation (6.4).

Only the resistance R of the steady state cases with a unit concentration constant in time (cases 19 to 27) is shown in Table 6.1.1. The reason is that the cases with unit inventory (cases 1 to 18) will give zero steady state concentrations because the inventory depletes with time. In comparing R with R_{SKB} in Table 6.1.1 one should be aware that equation 6.3 is only valid for cases 19-21 and 23-24 because only for these cases the pinhole is totally filled with water. For the remaining cases (22, 25-27) the term $R_{p/b}^{diff}$ is not valid and the results of the last two columns of the table show only the contribution of the first term in Equation (6.3) to R_{SKB}.

Cases 20 and 21 give, as expected, the same results as case 19 because the only differences in the input data is related to the sorption coefficient *Kd* which, for the steady state calculations, does not influence the results.

Table 6.1.1 *Steady state results for a source term of unit concentration for the pinhole interface calculations.*

Case	Canister inventory	Pinhole Area and Content	Bentonite buffer Diffusion	Bentonite buffer Sorption	$Flux_{p/b}$ (mole/s)	R	R_{SKB}[2]
19	UC	A1/PW	DM	KdM	2.02×10^{-14}	4.93×10^{13}	5.50×10^{13}
20	UC	A1/PW	DM	KdL	2.02×10^{-14}	4.93×10^{13}	5.50×10^{13}
21	UC	A1/PW	DM	KdH	2.02×10^{-14}	4.93×10^{13}	5.50×10^{13}
22	UC	A1/ PB	DM	KdM	2.61×10^{-15}	3.83×10^{14}	-
23	UC	A2/PW	DM	KdM	1.94×10^{-13}	4.93×10^{12}	6.74×10^{12}
24	UC	A3/PW	DM	KdM	1.59×10^{-12}	4.93×10^{11}	1.06×10^{11}
25	UC	A3/ PB	DM	KdM	2.52×10^{-13}	3.83×10^{12}	-
26	UC	A4/PB[1]	DM	KdM	1.22×10^{-12}	7.01×10^{11}	-
27	UC	A5/PB[1]	DM	KdM	2.91×10^{-12}	2.55×10^{11}	-

[1] 100% bentonite is assumed.

[2] Equation (6.3) is not valid for cases 22, 25 26 and 27 because the pinhole is partially or totally filled with bentonite (Neretnieks, 1986).

From the results in Table 6.1.1 of cases 19, 23 and 24 it is observed that the increase of the pinhole area by one order of magnitude corresponds to a flux increase of roughly the same magnitude. The pinhole resistance *R,* decreases exactly one order of magnitude. Case 22 has the same parameters as case 21 (see Table 2.1.2) but the pinhole is half-filled with bentonite, which results in a flux decrease of somewhat more than one order of magnitude. From case 26 to case27, both corresponding to pinholes completely filled with bentonite, the flux increases only by a factor of two, although the pinhole area increases by one order of magnitude. When the pinholes are half-filled the increase of flux is of the same order of magnitude as the ratio of the pinhole areas (cases 22 and 25).

Equation (6.3) used to compute the resistances of the compartment model is only valid for cases with a pinhole completely filled with water (Neretnieks, 1986).

The steady state resistances from three-dimensional and compartment modelling agree for cases 19, 20 and 21 but deviates for cases 24. The reason is that Equation (6.3) is derived for pinholes with small cross-section areas but for instance for case 24 that cross-section is already two orders of magnitude higher than for case 19.

Figures 6.1.1-6.1.4 show the steady state distribution of the solute in the canister, at the bentonite buffer and in the pinhole.

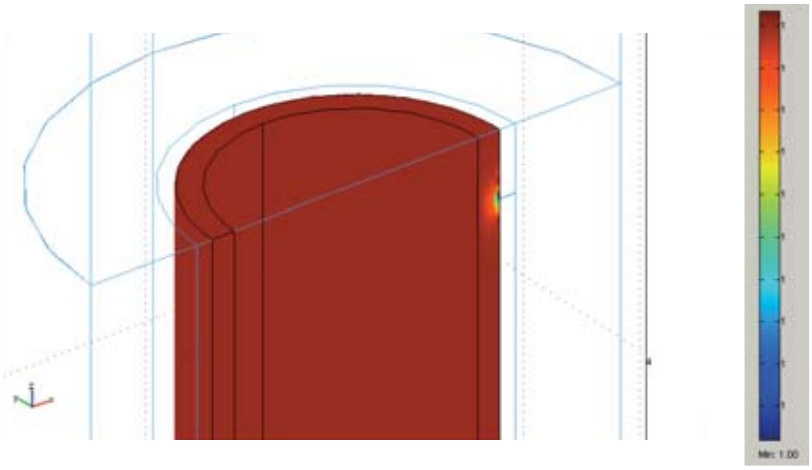

Figure 6.1.1 *The steady state distribution of the concentration at the source.*

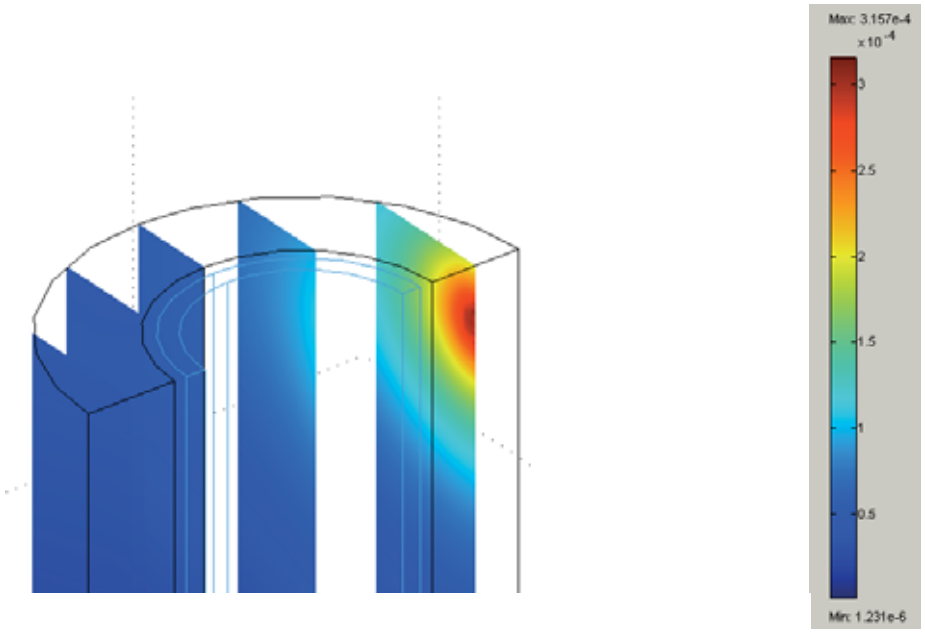

Figure 6.1.2 *The steady state distribution of concentration in the bentonite buffer around the canister.*

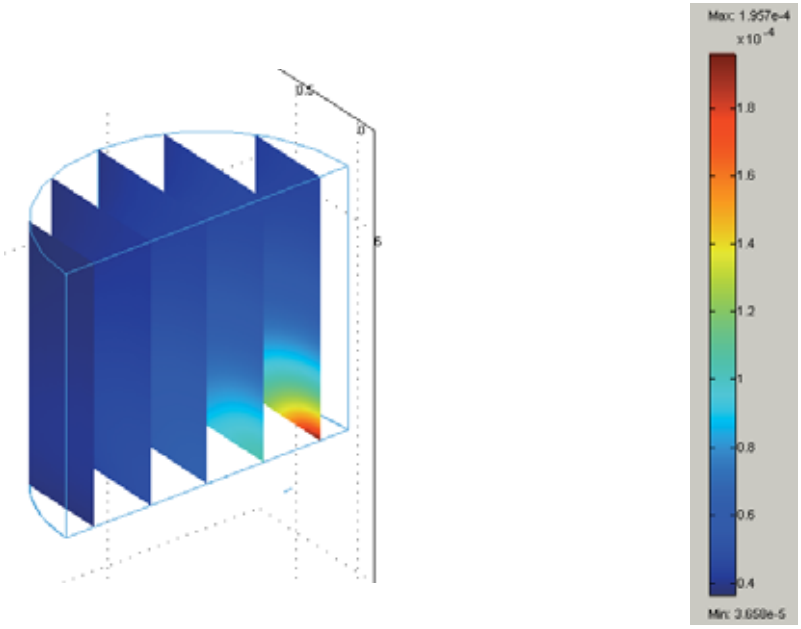

Figure 6.1.3 *The steady state distribution of concentration in the bentonite buffer above the canister.*

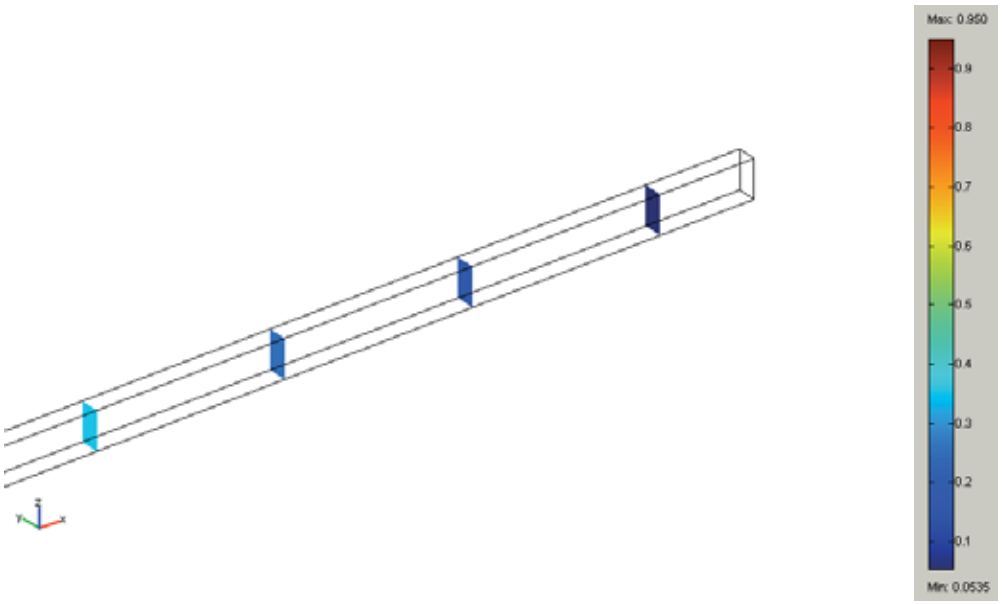

Figure 6.1.4 *The steady state distribution of concentration in the pinhole.*

6.1.2 Time dependent

For Case 19 the time-dependent calculations were done up to 10,000 years using the three dimensional FEM-model. The constant input concentration, the concentration at the outlet of the pinhole and the corresponding flux, are shown in Figures 6.1.5 and 6.1.6 respectively.

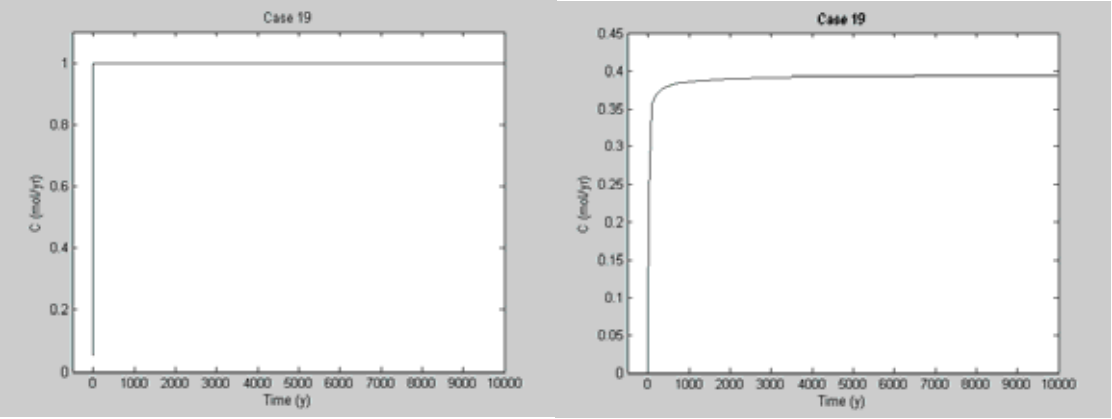

Figure 6.1.5 *The distribution of the constant input concentration in the canister (left picture) and the concentration at the outlet of the pinhole.*

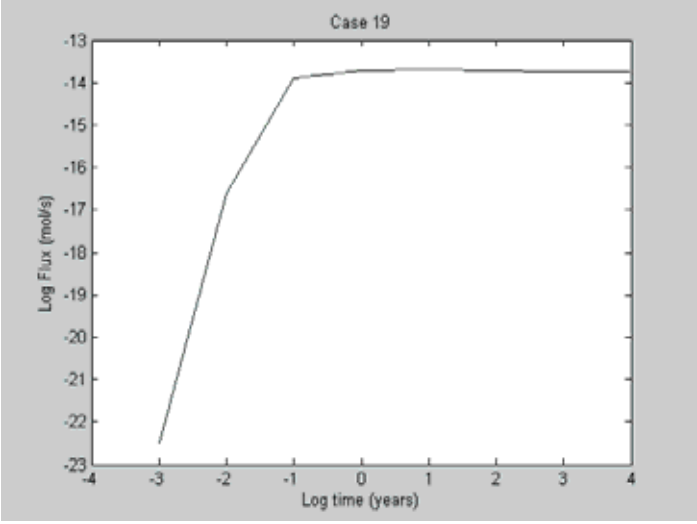

Figure 6.1.6 *The flux at the outlet of the pinhole.*

All breakthrough curves of fluxes versus time are shown in Figure A1 in Appendix I. Table 6.1.2 gives the fluxes at the outlet of the pinhole at 10,000 years. The resistance varies with time as the flux does as shown in Figure 6.1.7. Although the time steps are coarser up to one year, it can be observed that the resistance shows a maximum at early times and decreases somewhat later on. SKB's compartment models, based on the resistance approach use the steady state resistances, which are slightly conservative (se Table 6.1.1; log 5.50×10^{13}=13.7) with the exception of very early time points as shown by Figure 6.1.7.

Table 6.1.2 *Fluxes and resistances at the outlet of the pinhole at 10,000 years.*

Case	Canister	Pinhole Area	Pinhole Content	Bentonite buffer diffusion	Bentonite buffer Sorption	$Flux_{p/b}$ (mole/s)
1	UI	A1	PW	DM	KdM	1.91×10^{-14}
2	UI	A1	PW	DL	KdM	3.24×10^{-14}
3	UI	A1	PW	DH	KdM	1.90×10^{-14}
4	UI	A1	PW	DM	KdL	2.00×10^{-14}
5	UI	A1	PW	DM	KdH	2.51×10^{-14}
6	UI	A1	PB	DM	KdM	1.55×10^{-17}
7	UI	A1	PB	DL	KdM	1.55×10^{-18}
8	UI	A1	PB	DH	KdM	1.54×10^{-16}
9	UI	A1	PB	DM	KdL	1.22×10^{-15}
10	UI	A1	PB	DM	KdH	1.55×10^{-18}
11	UI	A2	PW	DM	KdM	2.84×10^{-14}
12	UI	A3	PW	DM	KdM	1.20×10^{-12}
13	UI	A4	PW	DM	KdM	1.21×10^{-14}
14	UI	A5	PW	DM	KdM	2.38×10^{-16}
15	UI	A2	PB	DM	KdM	1.54×10^{-16}
16	UI	A3	PB	DM	KdM	1.49×10^{-15}
17	UI	A4	PB[1]	DM	KdM	6.87×10^{-15}
18	UI	A5	PB[1]	DM	KdM	1.70×10^{-14}
19	UC	A1	PW	DM	KdM	1.23×10^{-14}
20	UC	A1	PW	DM	KdL	2.02×10^{-14}
21	UC	A1	PW	DM	KdH	2.51×10^{-14}
22	UC	A1	PB	DM	KdM	1.55×10^{-17}
23	UC	A2	PW	DM	KdM	2.87×10^{-14}
24	UC	A3	PW	DM	KdM	1.23×10^{-12}
25	UC	A3	PB	DM	KdM	1.50×10^{-15}
26	UC	A4	PB[1]	DM	KdM	6.88×10^{-15}
27	UC	A5	PB[1]	DM	KdM	1.72×10^{-14}

[1] 100% bentonite is assumed.

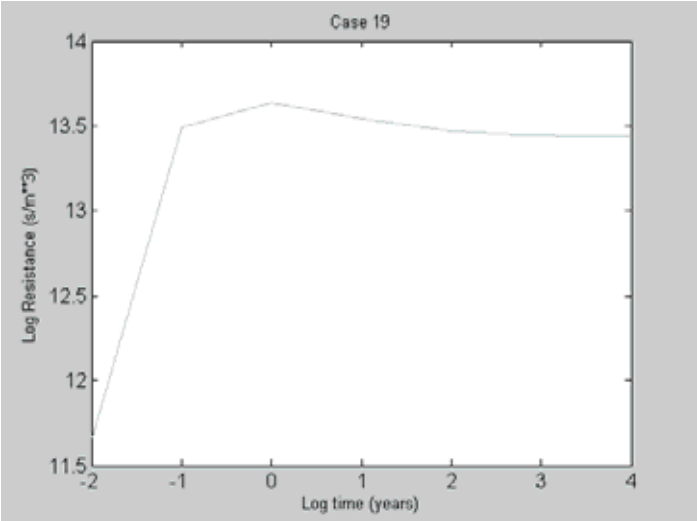

Figure 6.1.7 *The pinhole resistance versus time.*

As expected, the fluxes at 10,000 years are lower than at steady state (compare Table 6.1.2 with Table 6.1.1). For the calculation cases where the pinhole is partially full of bentonite this lowering can be as high as two orders of magnitude.

Because the fluxes at steady state are lower than the transient fluxes, the resistances at steady state are conservative when compared with the resistance at any time point, except at the early time points (up to 100 years in some cases, see the figure of flux versus time for the pinhole interface cases in Appendix I). Therefore Table 6.1.1 showing the resistance estimations for the steady state gives us the sufficient information on the resistance estimations for the pinhole interface cases.

6.2 Fracture Interface Calculations

6.2.1 Steady state

One should note that the solute first diffuses in the bentonite buffer around the canister before entering the fracture. After entering in the fracture, the solute is carried by advection and dispersion/diffusion to its outlet. Retardation is included in the bentonite buffer but not in the fracture. The fluxes are computed in the interface between the bentonite buffer and the fracture. The resistance at the fracture inlet is compared with the theoretical one used by resistance based compartment models.

Compartment modelling by SKB

The resistance between the bentonite buffer and the narrow surrounding fracture (Neretnieks, 1986) can be approximate by:

$$R_{b/f}^{Diff} = F\frac{\delta}{AD_{eff}^{bent}} \qquad (6.5)$$

where:
δ - is the fracture aperture,
A - is the fracture area,
F - is a geometrical factor,
D_{eff}^{bent} - is the effective diffusivity in the bentonite.

The limited capacity of the water flowing in the rock can be expressed (Neretnieks, 1986) by a resistance at the exit of the fracture equal as:

$$R^q = \frac{1}{A_q \sqrt{q}} \tag{6.6}$$

where:
q - is the water flux at the fracture,
A_q - is a lumped parameter depending on the geometrical properties of the fracture and on the diffusivity of the solute on the groundwater.

Three dimensional modelling

First we have calculated the steady state flow field in the fracture, using the Navier--Stockes equation. Once obtained that flow-field, which is given by the three components of the water velocity (u, v, and w)[2], we can use them in the transport equation that describes the migration of the solute in the fracture.

Figure 6.2.1 show the steady state streamlines around the canister.

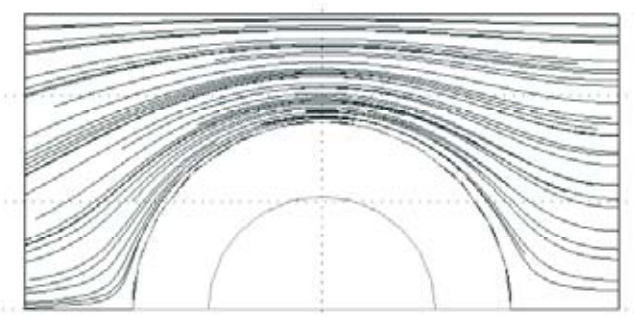

Figure 6.2.1 *Steady state streamlines in the fracture plane.*

Using the FEMLAB calculation we can compute the transport resistance R by evaluating the computed flux and the concentrations at the inlet and outlet of the fracture:

$$R = \frac{\Delta C}{\varphi} = \frac{C_1 - C_2}{\varphi} \tag{6.7}$$

[2] (u,v,w) is the standard notation for (x,y,z) in fluid mechanics and is also used by FEMLAB.

where:
C_1 - is the mean steady state concentration in the fracture (0.989803 mole/m^3),
C_2 - is the mean steady state concentration in the bentonite (0.07583 mole/m^3),
φ - is the flux at the interface (7.70488×10^{-11} mole/s).

Results of calculations

In this Section we describe in some detail one case calculation (case 26), to illustrate the approach used in this work.

The input parameters of case 26 are: diffusivity in water (3.2×10^{-3} m^2 y^{-1}), effective diffusivity in bentonite buffer (2.2×10^{-3} m^2 y^{-1}), Kd (0.1 m^3 kg^{-1}), Darcy velocity (2.0×10^{-3} m y^{-1}) and fracture porosity (1.5×10^{-4}). The pore velocity is calculated from the Darcy velocity assuming that one fracture takes all the flow for the canister. We obtain a flux at the entrance of the fracture equal to 7.70×10^{-11} mole/s. The corresponding concentration at that interface is 0.76 mole/m^3.

Inserting the value of $\frac{F\delta}{A} = 0.9$ given in Table I in (Hedin) in Equation (6.5), we obtain a resistance equal to 1.29×10^{10} (s/m^3).

This value should be compared with 1.19×10^{10} (s/m^3) obtained by FEMLAB using Equation (6.7). The resistance given by Equation (6.7) gives a result close to that of Equation (6.5).

The value of the resistance offered by the fracture to the flowing water R^q, is according to Equation (6.6) equal to 2.35×10^{10} (s/m^3).

The fracture inlet concentration is 0.762686 (mole/m^3) and the outlet concentration is 0.001375 (mole/m^3). The total flux at fracture outlet is 7.223725×10^{-11} mole/s and the resistance is therefore 1.05×10^{10} s/m^3. This resistance is two times lower than that of the corresponding compartment model.

The total resistance R_{SKB}=3.64×10^{10} (s/m^3) offered by the fracture is somewhat conservative for the compartment model approach compared to the 3D calculations value of R=2.24×10^{10} (s/m^3). Equations 6.5 and 6.6 are used by SKB to represent a parameterisation of the fracture resistance. However it is not trivial to confirm that it is correct to compare the empirical resistance formulas (see Equation. 6.7) to those deduced from the steady-state equations by Neretnieks (1986). The reason is that the empirical equation (Equation 6.7) is applied in our calculations, to a given geometry (see Fig. 6.2.1) and it is not easy to verify if the dimensions and form of our fracture geometry are in full consonance with the parameterisation given by the geometric factor A_q (Equation 6.6) deduced by Neretnieks. Therefore to verify the applicability of that parameterisation, one should compare directly the degree of agreement between fluxes obtained by using our FEM model and the SR-97 results.

Table 6.2.1 shows results of the steady state calculations of the fracture interface model. Only the steady state cases with a fixed concentration at the canister (cases 20 to 31) are

shown. The reason is that the cases an initial uniform concentration (cases 1 to 19) will give zero steady state concentrations because the inventory depletes with time. Figure 6.2.2 shows the concentration in the fracture.

Table 6.2.1 *Steady state results of fracture interface calculations with fixed concentration at the canister.*

Case	Canister / Bentonite buffer	Bentonite buffer Diffusion	Bentonite buffer Sorption	Darcy Velocity	Fracture Aperture	Flux (mole/s)	R (s/m^3)
20	CC	DM	KdM	VM	HM	1.21×10^{-11}	1.1×10^{11}
21	CC	DL	KdM	VM	HM	3.14×10^{-12}	3.6×10^{11}
22	CC	DH	KdM	VM	HM	2.31×10^{-11}	8.4×10^{10}
23	CC	DM	KdH	VM	HM	1.21×10^{-11}	1.1×10^{11}
24	CC	DM	KdM	VL2	HM	1.16×10^{-11}	1.2×10^{11}
25	CC	DM	KdM	VH2	HM	1.08×10^{-11}	1.2×10^{11}
26	CC	DM	KdM	VM	HL	7.70×10^{-11}	2.2×10^{10}
27	CC	DM	KdM	VL2	HL	5.80×10^{-11}	2.6×10^{11}
28	CC	DM	KdM	VH2	HL	1.00×10^{-10}	1.5×10^{10}
29	CC	DM	KdM	VM	HS	4.87×10^{-12}	3.9×10^{11}
30	CC	DM	KdM	VL2	HS	4.71×10^{-12}	4.1×10^{11}
31	CC	DM	KdM	VH2	HS	4.64×10^{-12}	4.3×10^{11}

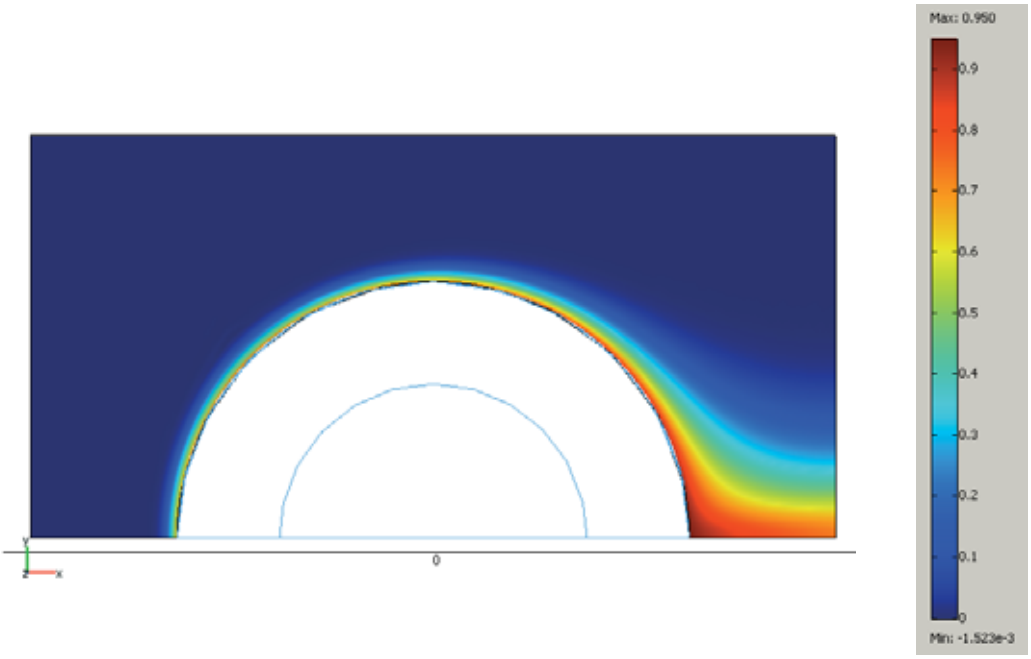

Figure 6.2.2 *Steady state concentration in the fracture.*

As expected, the variations of the sorption coefficient do not affect the flux of the steady state (see for instance case 20 versus case 23).

The only parameter that varies in cases 20, 21 and 22 is the effective diffusivity. A variation of two orders of magnitude between cases 21 and 22 results in a flux increase by a factor of 7 approximately.

Decreasing the Darcy velocity by a factor of 4 (cases 24 versus case 25) results in a very small variation of the flux at the fracture interface (around 7%) for the case of a fracture with an aperture of 0.1 mm. However if the fracture increases to 1mm (1 order of magnitude increase, cases 27 and 28) the flux decreases by a factor somewhat less than 2, if the Darcy velocity decreases by a factor of 4. For a very small fracture (0.01mm) that flux ratio is only 3.7%.

6.2.2 Time dependent

We have selected a subset of eleven cases from Table 2.2.2 to perform the time-dependent calculations. Five of those calculations are for an initial inventory of 1Bq/m^3 and the remaining six cases are for a fixed concentration of 1Bq/m^3. These cases represent solubility-limited nuclides. The reason of using this subset of calculations is of practical nature; the calculations are time consuming and the information obtained by eleven cases instead of thirty-one, is sufficient for our purposes.

We use Case 26 to illustrate how the time-dependent calculations were conducted. All time-dependent calculations were carried out up to 10,000 years. The flux breakthrough curve of case 26 is shown at left in Figure 6.2.3.

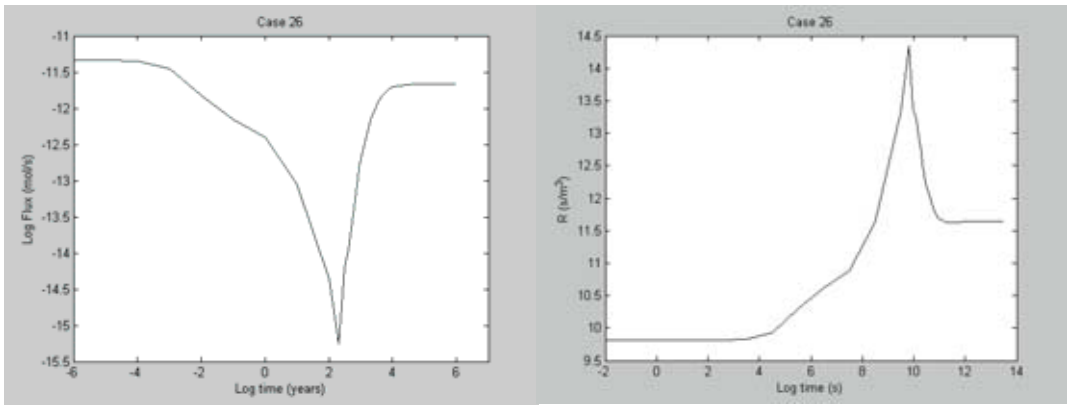

Figure 6.2.3 *Flux and resistance at the inlet of the fracture versus time (left and right pictures respectively).*

This figure shows an interesting feature. The flux at the very early time points is constant and then decreases to a minimum at 200 years to increase again. At early time points the flux is 6.0×10^{-12} (mole/s). The value of the flux at 10,000 years is 2.3×10^{-12} (mole/s) and at 1,000,000 years (not shown in the figure) it is 2.5×10^{-12} (mole/s). This

feature will be investigated further because it may be of potential importance for the migration of nuclides with short half-life.

At very early time points the concentration gradient is high because there is a very small amount of solute in the fracture and the flux is relatively high. Slowly, a concentration is built up in the fracture, the resistance becomes higher and the flux decreases until it reaches its minimum at 200 years. Meanwhile the water flow in the fracture carries away the "excess" of solute and the flux starts increasing again until it reaches a stable value. Therefore if the diffusivity in the bentonite buffer increases the depth of the flux curve should increase. It is what we can observe comparing the figure of case 22 (DH $=2.2\times10^{-2}$ m^2 y^{-1}) with that of case 20 (DM $=2.2\times10^{-3}$ m^2 y^{-1}) in Appendix I, Figure A2; for these cases all parameters are equal except the diffusivity.

The fluxes at the inlet of the fracture, at 10,000 years, are shown in Table 6.2.3. The breakthrough curves are shown in Figure A2 in the Appendix I. One should observe that the breakthrough curves for the cases having an unit inventory in the bentonite buffer (cases 1 to 19 of Table 2.2.2), do not, in contrast to the solubility limited cases, show a deepening on the flux at 200 years (see for instance cases 1 to 7 of Figure A2 in the Appendix I).

The resistance that the nuclides are subjected to when they leave the bentonite buffer and enter in the fracture is shown at right in Figure 6.2.3. One should observe that the time scale of that picture is in seconds, not in years, because the top of the resistance curve has a smaller spread than that of the corresponding concentration profile and would make the picture difficult to interpret with another time scale. The maximum of curve occurs at circa 200 years, as the minimum of the flux curve does.

Table 6.2.3 *Fluxes on the fracture interface at 10,000 years for some transient calculations.*

Case	Canister / Bentonite buffer	Bentonite buffer Diffusion	Bentonite buffer Sorption	Darcy Velocity	Fracture Aperture	Flux
1	BI	DM	KdM	VM	HM	4.67×10^{-13}
3	BI	DH	KdM	VM	HM	8.16×10^{-13}
4	BI	DM	KdL	VM	HM	5.42×10^{-12}
6	BI	DM	KdM	VL2	HM	4.27×10^{-13}
7	BI	DM	KdM	VL10	HM	6.13×10^{-13}
20	CC	DM	KdM	VM	HM	3.70×10^{-11}
22	CC	DH	KdM	VM	HM	1.91×10^{-12}
24	CC	DM	KdM	VL2	HM	1.45×10^{-11}
26	CC	DM	KdM	VM	HL	1.97×10^{-12}
27	CC	DM	KdM	VL2	HL	1.94×10^{-12}
28	CC	DM	KdM	VH2	HL	2.00×10^{-12}

7 Conclusions

Although 3D modelling using finite-elements is memory- and CPU intensive, we can conclude that it exists already general commercial packages for finite-element modelling with the required ability to solve PDE's describing different physical and chemical phenomena that can be coupled with each other. Therefore, due to advances in computer technology, FEM-modelling is becoming a realistic approach to model coupled flow and transport processes in the near field.

7.1 Pinhole Interface

For a small corrosion hole in a KBS-3 type of canister with a cross-section area, not larger than about 10^{-4} m^2, it is concluded that the concept of transport resistance (used by SKB in their compartment models) can describe accurately the mass-transfer process, when compared with the results obtained by a 3D FEM-model describing the same geometry. For pinholes with larger cross-section areas the resistance method is somewhat conservative.

7.2 Fracture interface

Migration of nuclides into a near-field fracture using the resistance concept cannot be described in an entirely satisfactory way during a short transient period of around 200 years (for the parameters studied in this report). The reason is that the formulas used in the transport resistance approach are based on the solution of a steady-state equation. However, for the steady state regime of the fracture interface model, the method is still quite satisfactory although more conservative than for the case of the model describing the interface between pinhole and bentonite buffer

On the other hand the migration of short-lived nuclides in the near field may require a more detailed estimation than that allowed by the transport resistance approach. To obtain definitive conclusions on mass transfer in the fracture, it is necessary to integrate both finite-element models (which goal has been to analyse the mass transfer processes separately) into a single integrated model and to compare the results directly with the SKB's breakthrough curves for some specific nuclides.

References

Hedin A (2002). Integrated Analytic Radionuclide Transport Model for a Spent Nuclear Fuel Repository in Saturated Fractured Rock. Nuclear Technology 138 pp 79-205.

Lindgren M and Lindström F (1999). SR97 Radionuclide Transport Calculations. SKB report TR-99-23.

Neretnieks I (1986). Stationary Transport of Dissolved Species in the Backfill Surrounding a Waste Canister in Fissured Rock: Some Simple Analytical Solutions. Nuclear Technology 72, pp 194-200.

SKI/SSI (2003). AMBER and Ecolego Intercomparisions using Calculations from SR 97., P., Robinson, P., Avila, R., Broed, R., Pereira A. and Xu, S., SKI/SSI Report 2003:8/2003:11.

SKB (1999). Deep Repository for Spent Fuel. SR 97- Post-closure safety, volumes I and II. SKB report TR-99-06.

SKB (1998). Equivalent flow rate concept used in near field transport model COMP23 – Proposed values for SR 97. SKB report R-98-53.

Acknowledgement

Parallel Dator Center (PDC) at KTH has given us the opportunity to use a supercomputer to perform the calculations presented in this report. We acknowledge PDC for the computer resources put at our disposition.

Our acknowledgement goes also to the proponents of the calculation cases, Peter Robinson and Philip Maul, from Quintessa Ltd.

Appendix I

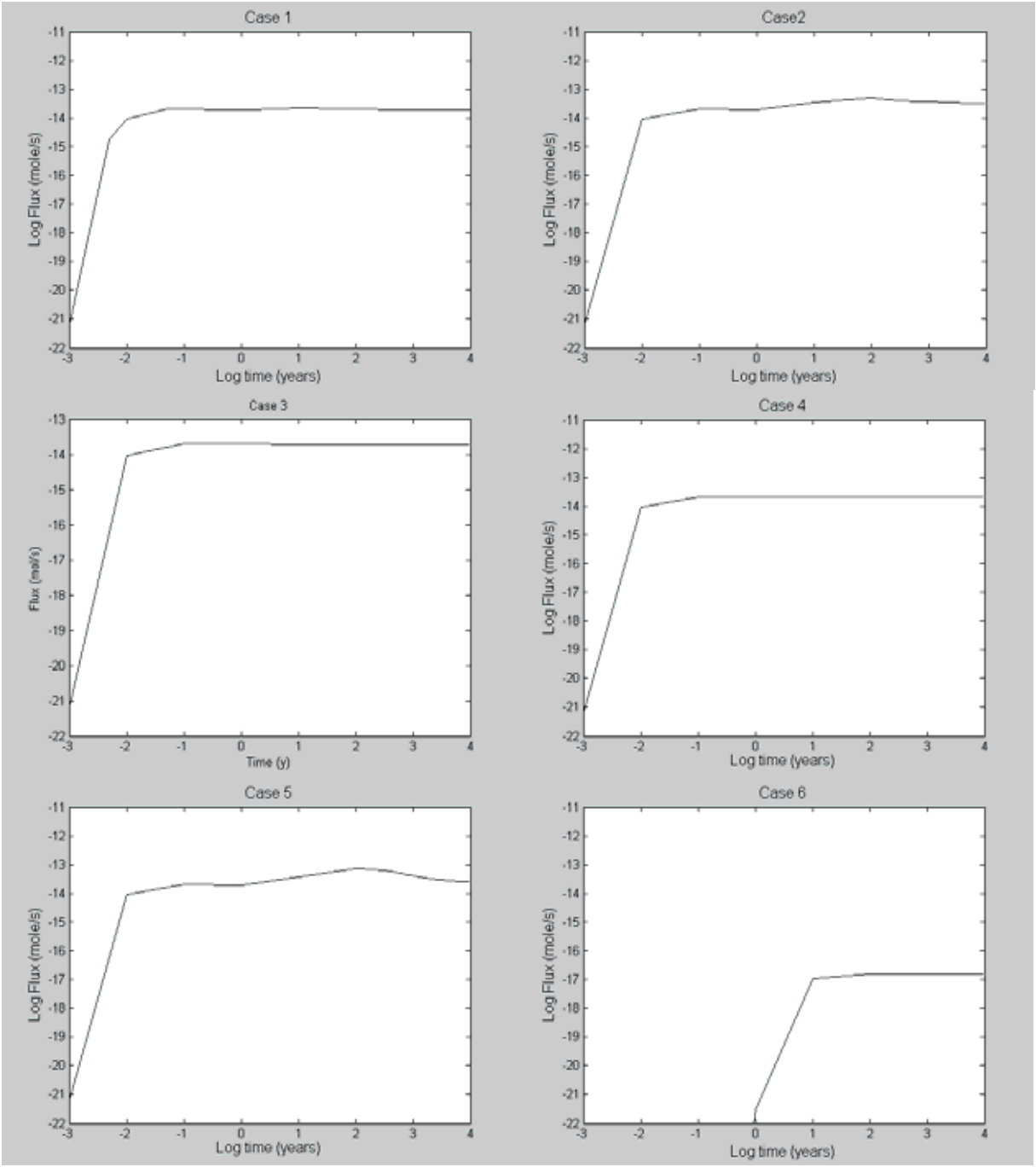

Figure A.1 *Flux versus time at the outlet of the pinhole for a unit inventory source term.*

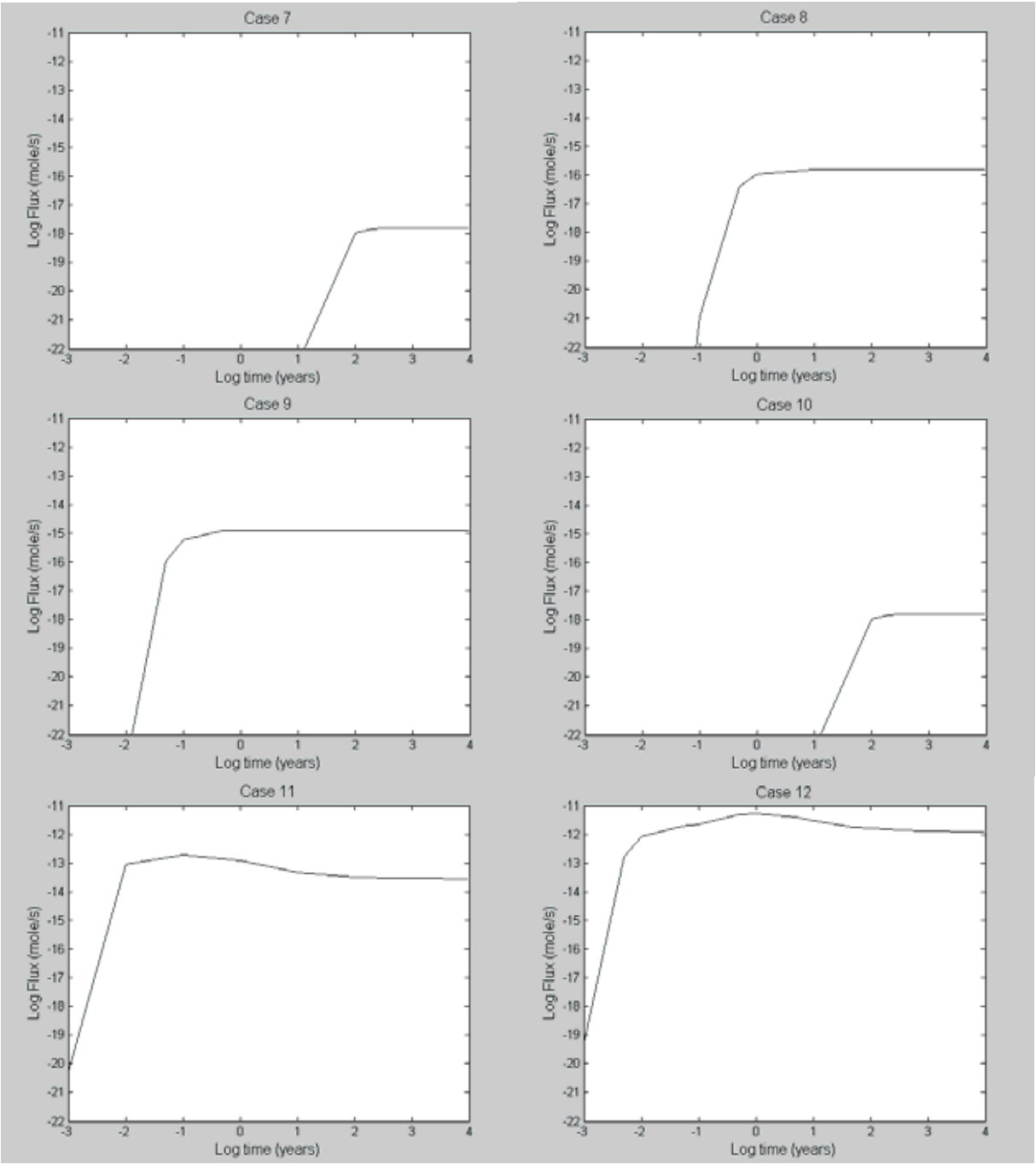

Figure A.1 (cont.) *Flux versus time at outlet of the pinhole for a unit inventory source term.*

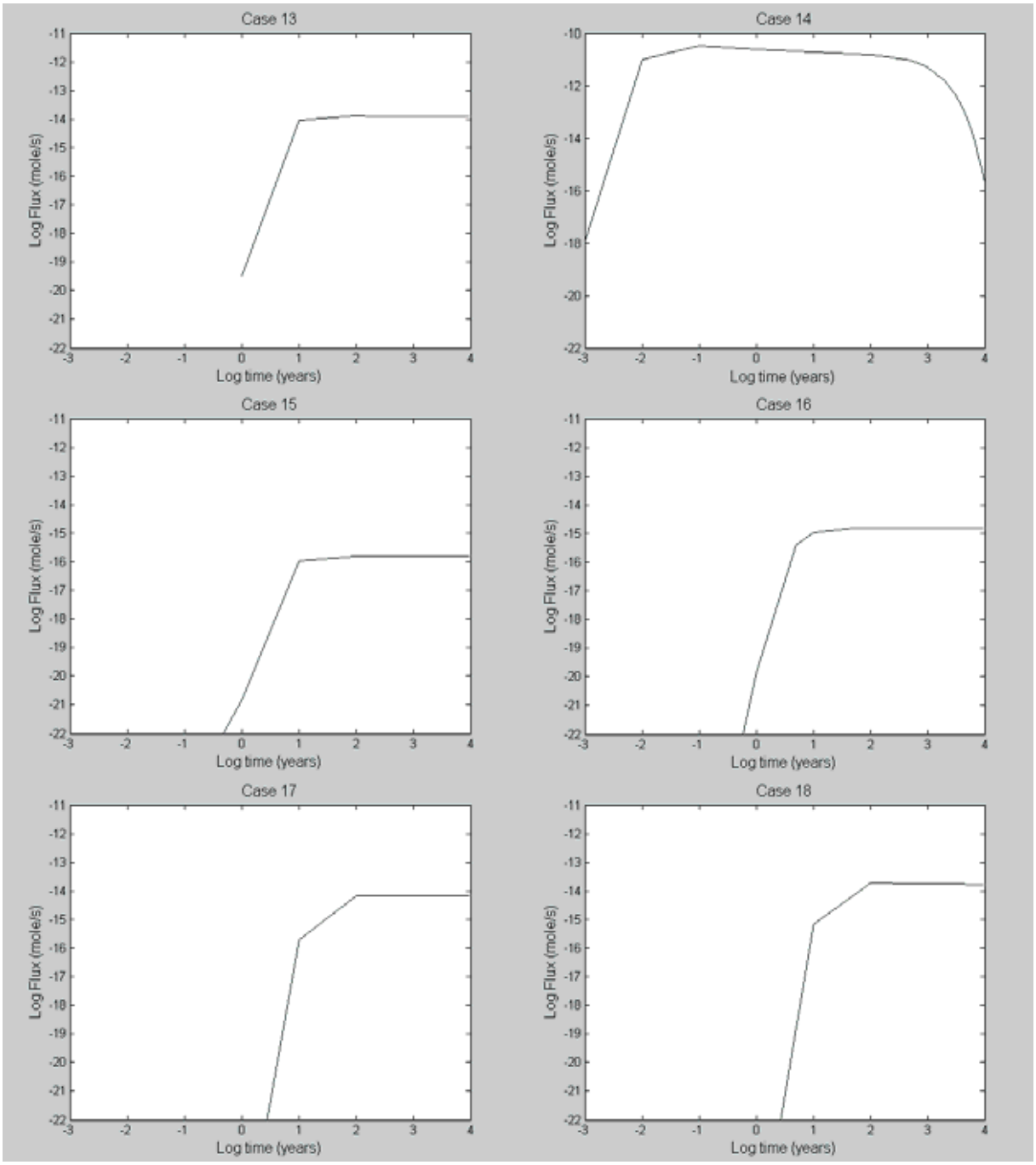

Figure A.1 (cont.) *Flux versus time at outlet of the pinhole for a unit inventory source term.*

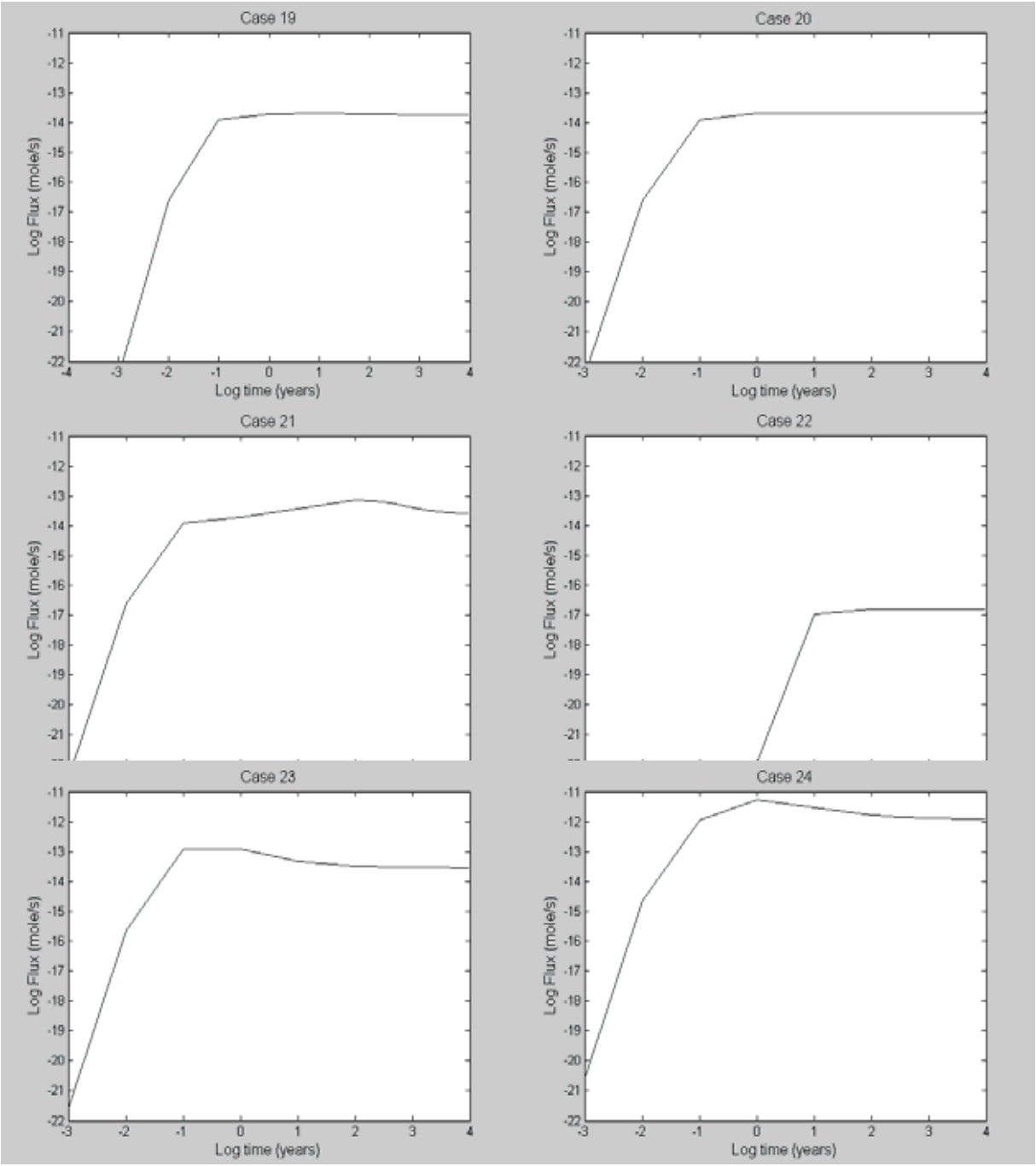

Figure A.1 (cont.) *Flux versus time at outlet of the pinhole for a unit inventory source term.*

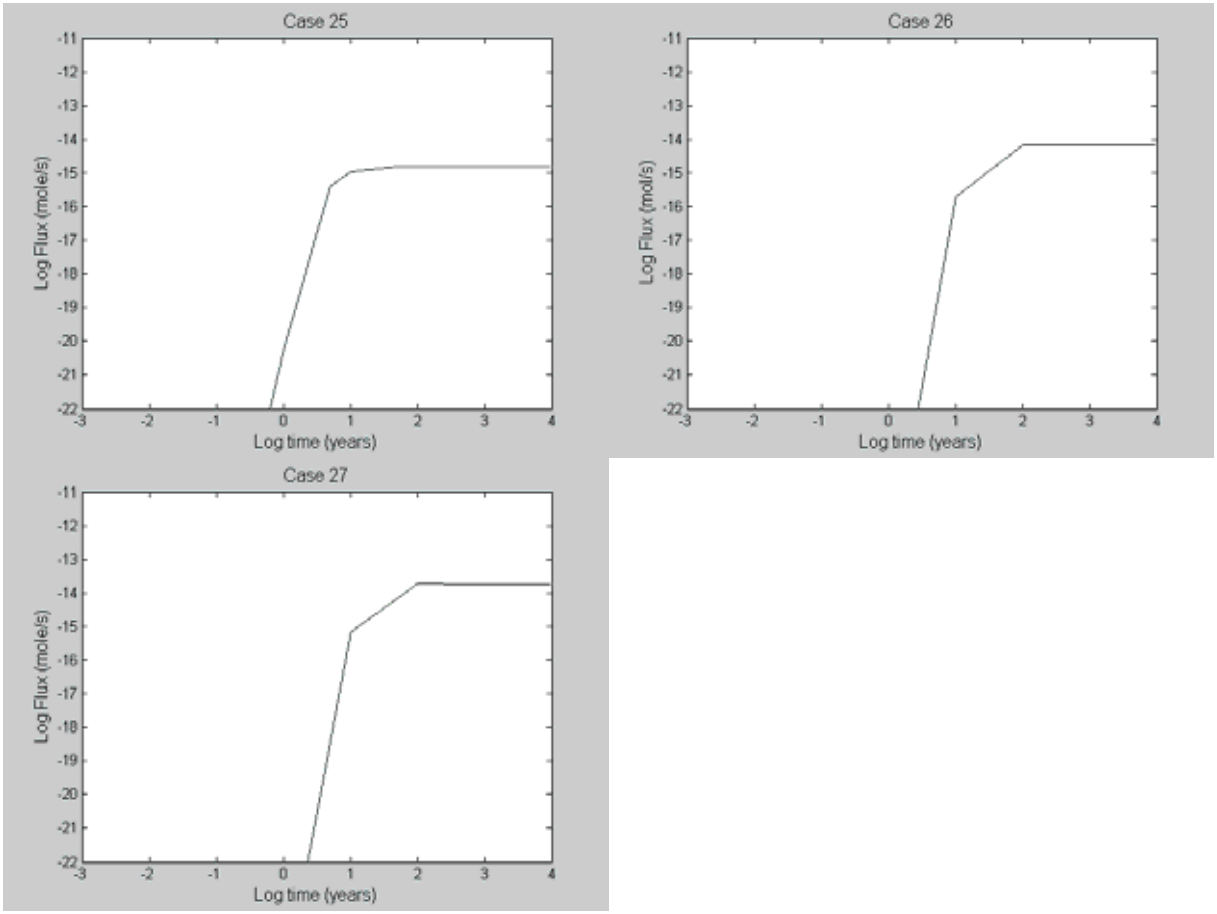

Figure A.1 (cont.) *Flux versus time at outlet of the pinhole for a unit inventory source term.*

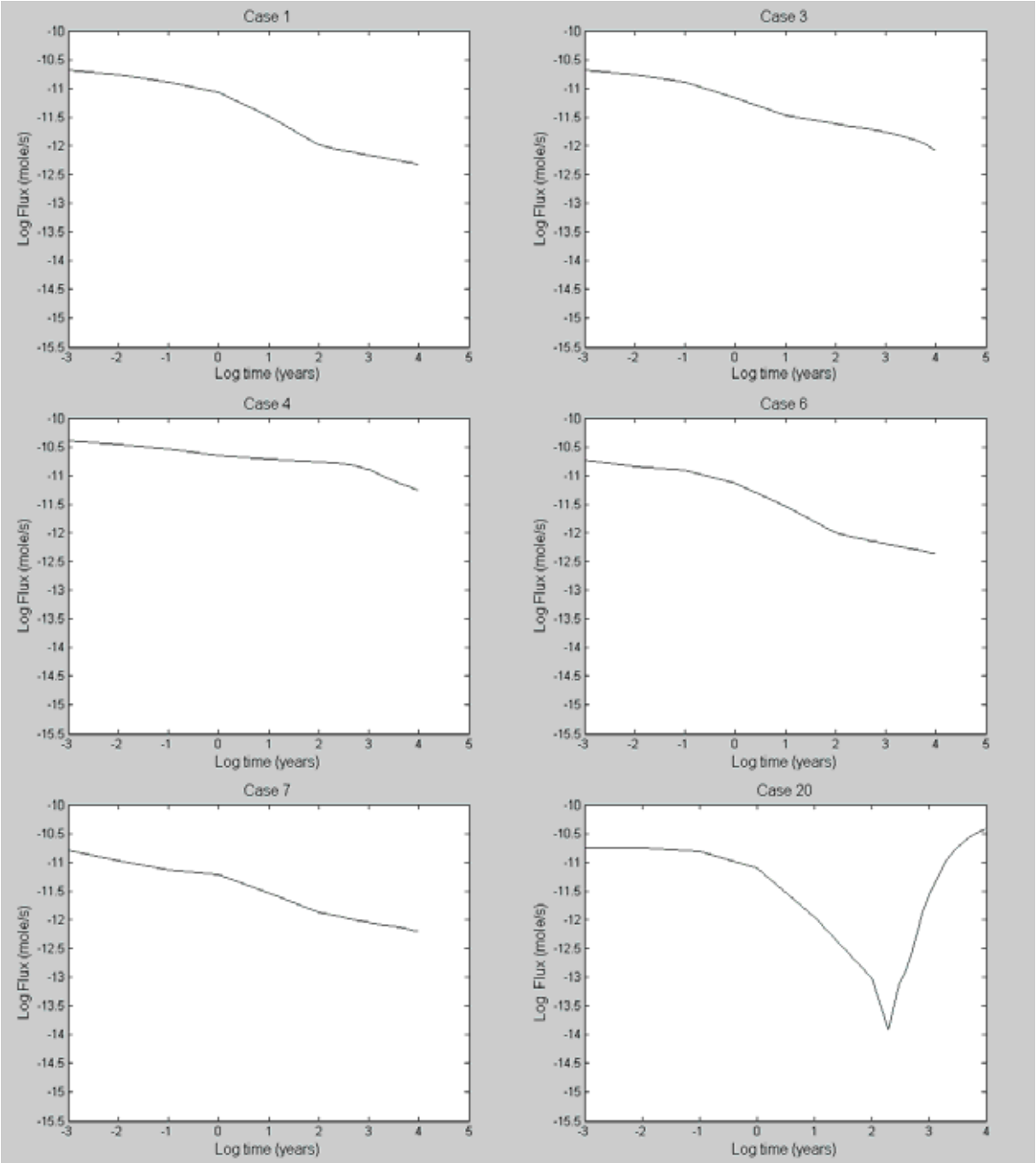

Figure A.2 *Flux versus time at the inlet of the fracture for a unit concentration source term.*

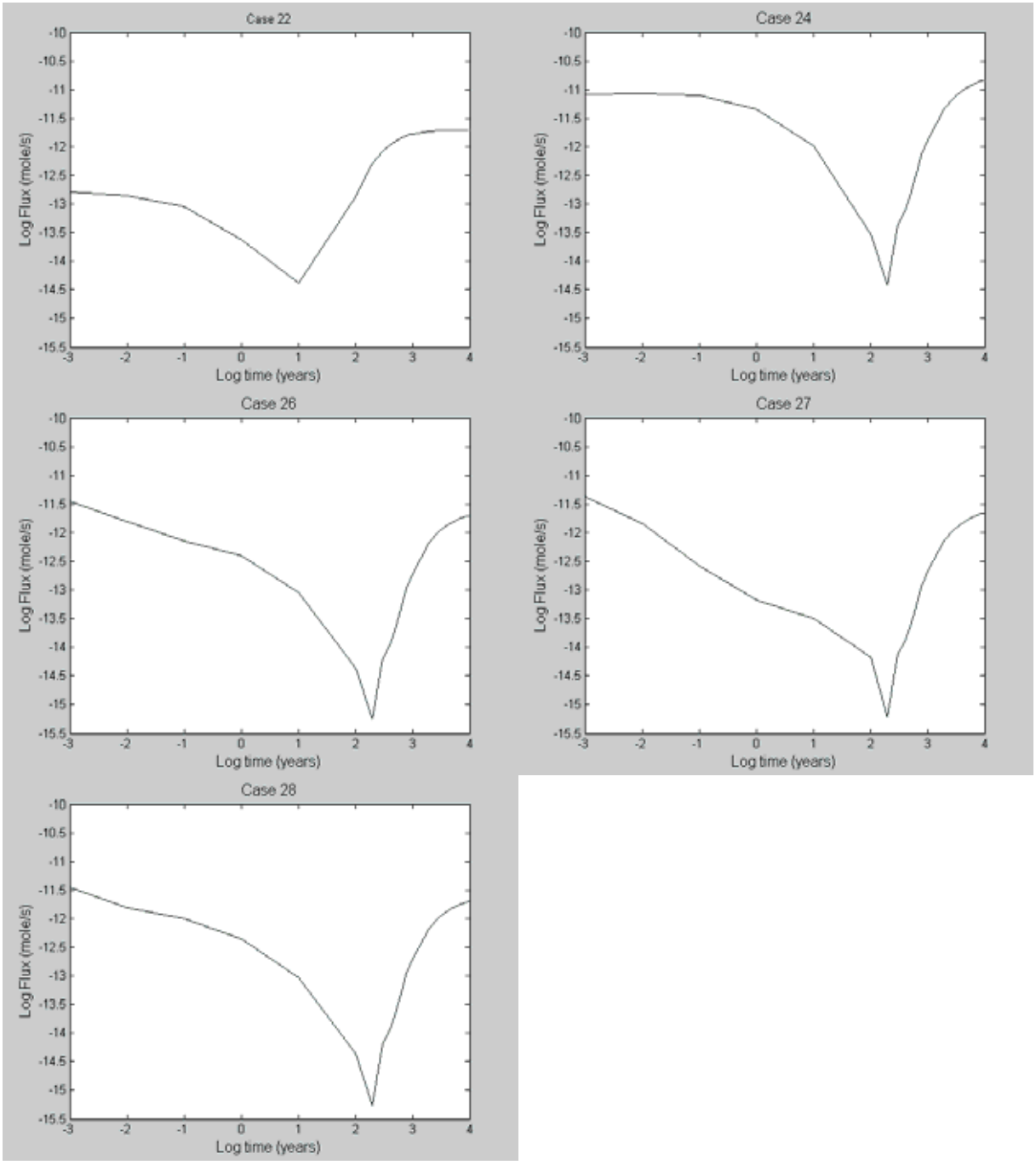

Figure A.2 (cont.) *Flux versus time at the inlet of the fracture for a unit concentration source term.*

Appendix II

Table A1 *The physical dimensions of the near field barrier system.*

Canister height (m)	4.833
Canister outer diameter (m)	1.050
Canister inner diameter (m)	0.95
Fuel gap volume (m^3)	1
Diameter of the bentonite buffer (m)	1.75
Height of the bentonite buffer (m)	6.833
Pinhole cross-section area (m^2)	1×10^{-6}, 1×10^{-5}, 1×10^{-4}, 1×10^{-3}, 1×10^{-2}
Fracture aperture (m)	1×10^{-5}, 1×10^{-4}, 1×10^{-3}
Fracture length (m)	2.75
Fracture with (m)	2.75

www.ski.se

STATENS KÄRNKRAFTINSPEKTION
Swedish Nuclear Power Inspectorate

POST/POSTAL ADDRESS SE-106 58 Stockholm
BESÖK/OFFICE Klarabergsviadukten 90
TELEFON/TELEPHONE +46 (0)8 698 84 00
TELEFAX +46 (0)8 661 90 86
E-POST/E-MAIL ski@ski.se
WEBBPLATS/WEB SITE www.ski.se